© 2020. Published by The Company of Biologists Ltd | Journal of Cell Science (2020) 133, jcs239491. doi:10.1242/jcs.239491

RESEARCH ARTICLE

STIM1 interacts with termini of Orai channels in a sequential manner

Liling Niu[1,2,*], Fuyun Wu[2,3,*], Kaili Li[4], Jing Li[2], Shenyuan L. Zhang[5,‡], Junjie Hu[2,4,‡] and Qian Wang[1,‡]

ABSTRACT

Store-operated Ca^{2+} entry (SOCE) is critical for numerous Ca^{2+}-related processes. The activation of SOCE requires engagement between stromal interaction molecule 1 (STIM1) molecules on the endoplasmic reticulum and Ca^{2+} release-activated channel (CRAC) Orai on the plasma membrane. However, the molecular details of their interactions remain elusive. Here, we analyzed STIM1-Orai interactions using synthetic peptides derived from the N- and C-termini of Orai channels (Orai-NT and Orai-CT, respectively) and purified fragments of STIM1. The binding of STIM1 to Orai-NT is hydrophilic based, whereas binding to the Orai-CT is mostly hydrophobic. STIM1 decreases its affinity for Orai-CT when Orai-NT is present, supporting a stepwise interaction. Orai3-CT exhibits stronger binding to STIM1 than Orai1-CT, largely due to the shortness of one helical turn. The role of newly identified residues was confirmed by co-immunoprecipitation and Ca^{2+} imaging using full-length molecules. Our results provide important insight into CRAC gating by STIM1.

KEY WORDS: Store-operated Ca^{2+} entry, CRAC, STIM1, Gating mechanism, Immunodeficiency

INTRODUCTION

Intracellular Ca^{2+} is mostly stored in the endoplasmic reticulum (ER). When the Ca^{2+} store is depleted by either blockage of the ER-resident Ca^{2+} pump or opening of the Ca^{2+} channel, a cascade of events termed store-operated Ca^{2+} entry (SOCE) is triggered (Hogan and Rao, 2015; Prakriya and Lewis, 2015; Putney, 1986). ER-localized stromal interaction molecule 1 (STIM1) senses Ca^{2+} depletion in the ER (Liou et al., 2005; Roos et al., 2005; Zhang et al., 2005), migrates to the ER-plasma membrane (PM) junctions (Baba et al., 2006; Liou et al., 2007; Luik et al., 2006; Wu et al., 2006) and activates PM-embedded Ca^{2+} release-activated channel (CRAC) Orai1 (Feske et al., 2006; Lunz et al., 2019; Prakriya et al., 2006; Vig et al., 2006; Yeromin et al., 2006; Zhang et al., 2006; Zhou et al., 2017), thereby allowing Ca^{2+} influx. The entry of Ca^{2+} could be used to replenish the ER Ca^{2+} store, but more often it boosts cytosolic Ca^{2+} concentrations quickly to achieve certain signaling events. STIM-Orai-mediated activity is commonly seen during immune cell activation. As a result, loss-of-function mutations in STIM1 or Orai1 in humans are linked to immunodeficiency (Feske et al., 2010; Lacruz and Feske, 2015; Prakriya and Lewis, 2015).

Orai is composed of four transmembrane (TM) segments (TM1–TM4) with both termini facing the cytosol. Structural analysis of *Drosophila* Orai (also known as olf186-F; dmOrai) has revealed that the protein forms a hexamer (Hou et al., 2018, 2012; Liu et al., 2019). The ion pore is generated by six TM1s from the hexamer, which extend into the cytosol as continuous helices using the N-terminus (NT) of Orai. A glutamate (E106 in human Orai1) in the TM1 near the extracellular end ensures ion selectivity (Hou et al., 2012; Prakriya et al., 2006; Vig et al., 2006; Yamashita et al., 2007; Yeromin et al., 2006). The C-terminus (CT) of Orai, which becomes a helical extension of TM4, bends and pairs into three anti-parallel coiled coils (CCs) in the hexamer (Hou et al., 2012), but straightens in the open state (Hou et al., 2018; Liu et al., 2019). Mutations in this region, such as L273S, are known to compromise STIM recruitment (Frischauf et al., 2009; Muik et al., 2008).

STIM uses a single TM to span the ER membrane. The luminal side of STIM folds into a Ca^{2+}-sensing module with two EF hands and a sterile α-motif (SAM) domain (Gudlur et al., 2018; Soboloff et al., 2012; Zheng et al., 2018a). Release of Ca^{2+} caused by store depletion triggers conformational changes that can be passed onto the cytosolic side (Enomoto et al., 2019). The first half of the cytosolic portion of STIM appears mostly as a helical pattern and assembles into three CCs (Hogan et al., 2010; Prakriya and Lewis, 2015). These CCs tend to form dimers and likely rearrange during activation (Covington et al., 2010; Hirve et al., 2018; Ma et al., 2015; Muik et al., 2009). The second half ends with a polybasic region that anchors the protein to the negatively charged plasma membrane (Calloway et al., 2011; Korzeniowski et al., 2009; Liou et al., 2007; Park et al., 2009; Walsh et al., 2010).

Interactions between STIM and Orai are fundamental to successful SOCE and, therefore, have attracted considerable attention. However, their interface has not been analyzed systematically (Böhm and Laporte, 2018; Zhou et al., 2017), likely due to difficulties purifying full-length molecules, let alone setting up complexes. The TM4 extension, i.e. the CT of Orai, is thought to recruit STIM. Nevertheless, the TM1 extension (NT) would be equally important, as it connects to the ion pore and must be moved during Orai activation (Derler et al., 2018; Liu et al., 2019; Yamashita et al., 2020; Zhou et al., 2016). On the STIM side, the minimal fragments for Orai activation have been determined to be the CRAC-activating domain (CAD; residues 342–448) (Park et al., 2009) or the STIM-Orai activating region (SOAR; residues 344–442) (Yuan et al., 2009), both of which include CC2 and CC3. When tandem CAD/SOAR is attached to the CT of Orai, the chimeric construct becomes constitutively active (Böhm and Laporte, 2018; Butorac et al., 2019; Li et al., 2011; Prakriya and Lewis, 2015; Zheng et al., 2018a; Zhou et al., 2017).

[1]Department of Immunology, School of Basic Medical Sciences, Tianjin Medical University, and Tianjin Key Laboratory of Cellular and Molecular Immunology, Tianjin 300070, China. [2]Department of Genetics and Cell Biology, College of Life Sciences, Nankai University, Tianjin 300071, China. [3]School of Basic Medical Sciences, Hubei University of Medicine, Shiyan 442000, China. [4]National Laboratory of Biomacromolecules, CAS Center for Excellence in Biomacromolecules, Institute of Biophysics, Chinese Academy of Sciences, Beijing 100101, China. [5]Department of Medical Physiology, College of Medicine, Texas A&M Health Science Center, Temple, TX 76504, USA.
*These authors contributed equally to this work

‡Authors for correspondence (huj@ibp.ac.cn; wangq@tmu.edu.cn; shenyuan.zhang@medicine.tamhsc.edu)

L.N., 0000-0002-4938-5517; J.L., 0000-0001-5844-936X; J.H., 0000-0003-4712-2243

Received 23 September 2019; Accepted 24 February 2020

Journal of Cell Science (2020) 133, jcs239491. doi:10.1242/jcs.239491

Three Orai and two STIM forms exist in mammals, with Orai1 and STIM1 being the most-studied molecules. Here, we utilized synthetic peptides of the NT and CT of Orai1 and Orai3 and purified fragments of STIM1 to systematically decode the determinants of STIM-Orai interactions. Our results reveal key residues and support the notion that STIM1 engages the CT first, and then acts on the NT for Orai pore opening.

RESULTS

Interactions between STIM1 and Orai termini

To study STIM1-Orai interactions, N-terminal biotinylated peptides derived from the sequences of both the NT and CT of human Orai1 and Orai3 were synthesized (Fig. 1A). The length for these peptides was chosen by previous truncation analysis (Zhang et al., 2011) and cytosolic exposure based on structural prediction (Hou et al., 2012; Stathopulos et al., 2013). To obtain a stable and Orai-interacting STIM1 fragment, we tested numerous constructs, all including the CAD/SOAR region, but with varied flanking sequences. Consistent with a previous report (Zhou et al., 2010), fragments ending at residue 531 behaved well during expression and purification (Fig. 1A). Peptides were incubated first with Flag-tagged STIM1 (residues 342–531), then bound to streptavidin-conjugated beads and the precipitated samples were resolved by SDS-PAGE. Western blot analysis using anti-Flag antibodies demonstrated that STIM1 co-precipitated with the NTs of both Orai1 (1NT) and Orai3 (3NT) (Fig. 1B, lanes 2 and 3). The CTs of both Orai1 (1CT) and Orai3 (3CT) also pulled down STIM1 (Fig. 1B, lanes 4 and 5). The amounts of bound STIM1 were higher with CTs than NTs (Fig. 1B, lanes 2, 3 vs 4, 5), and higher with 3CT than 1CT (Fig. 1B, lanes 4 vs 5). Negligible binding of STIM1 was observed when no peptide

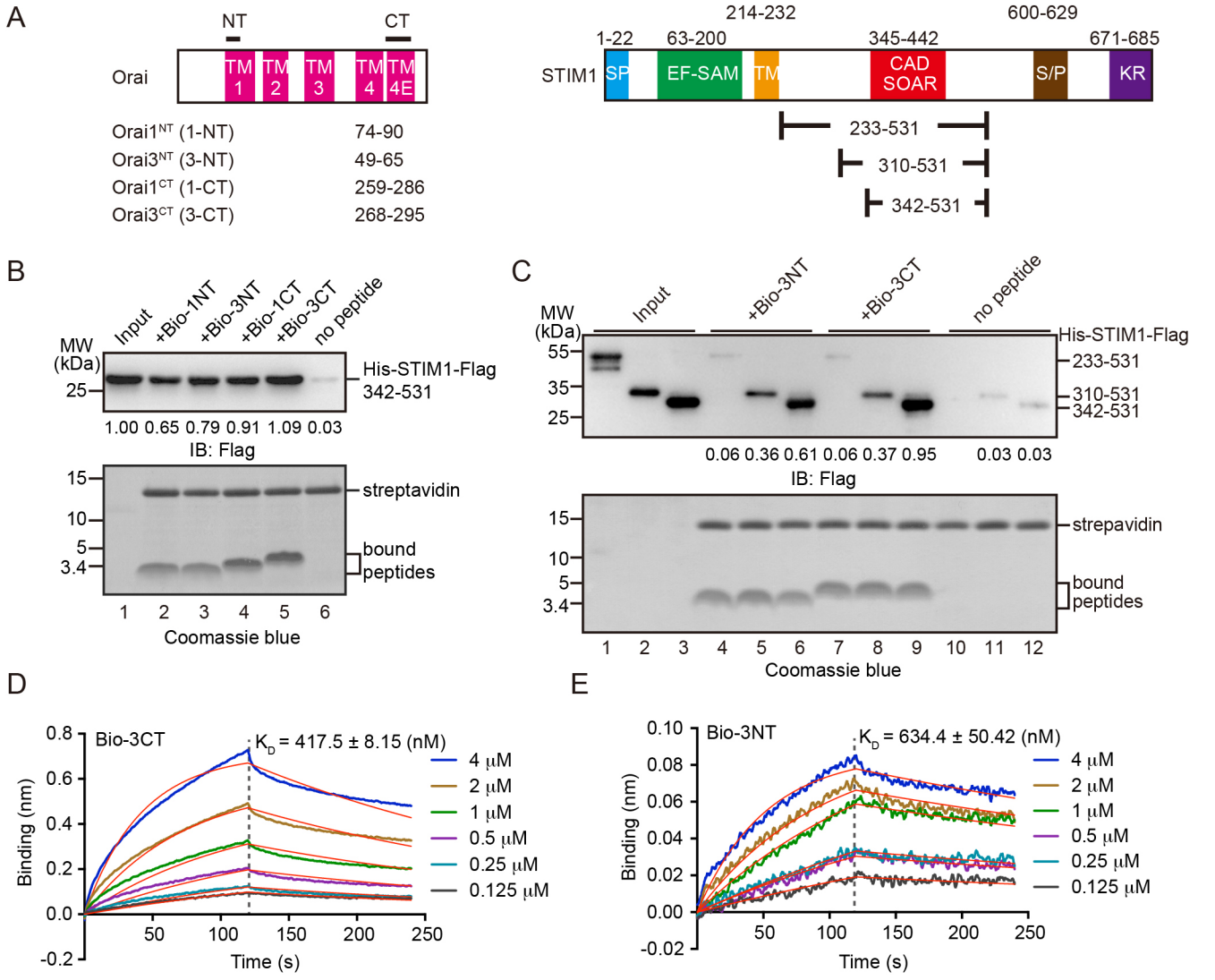

Fig. 1. Interactions between STIM1 and Orai termini. (A) Domain structures of Orai (left) and STIM1 (right). (B) Biotinylated Orai peptides (1NT, 1CT, 3NT, 3CT) were assayed for binding to STIM1 (residues 342–531) in streptavidin-based peptide pull-down assay. Precipitates were resolved by SDS-PAGE and detected by Coomassie Blue staining or western blotting using anti-Flag antibodies. 5% of the input and 50% of the precipitates were loaded. The relative levels of STIM1 were quantified using Gel-Pro analyzer software. MW, molecular mass (in all figures). Data are representative of three biological repeats. (C) As in B, but with different fragments of STIM1. The relative levels of precipitated STIM1 were normalized to the input correspondingly. Data are representative of three biological repeats. (D,E) Biolayer interferometry (BLI) analysis of STIM1 (residues 342–531) binding to Bio-3CT (D) and Bio-3NT (E). Biotinylated peptides were immobilized to streptavidin sensors. A gradient concentration of 0.125–4 µM STIM1 protein was used. Reference-subtracted raw data are rendered with fits (red lines) to a global 1:1 association-then-dissociation model. Association and dissociation phases were 120 s in length. Dissociation (K_D) constant is shown. Data are representative of three biological repeats.

Journal of Cell Science (2020) 133, jcs239491. doi:10.1242/jcs.239491

was added (Fig. 1B, lane 6), and equal amounts of bound peptides were revealed by Coomassie Blue staining (Fig. 1B, lower panel). These results confirmed that both the NT and CT of Orai channels engage STIM1, and suggest that 3CT binds more strongly to STIM1 than the NTs and 1CT. We thus selected Orai3 peptides for subsequent interaction analysis.

We also performed reverse pull-down, in which His-tagged STIM1 (residues 342–531) was immobilized by Ni-NTA beads and incubated with Orai peptides. As expected, both 3NT and 3CT peptides were efficiently pulled down by STIM1 (Fig. S1A). Notably, the biotinylation of the peptides had no impact on the interaction, as both types of peptides interacted equally with STIM1 (Fig. S1A). We then tested whether the interactions are sensitive to Ca^{2+}. No prominent changes were observed when 2 µM Ca^{2+} or 2 µM EDTA was added to the pull-down assay (Fig. S1B).

We further tested whether different fragments of STIM1 exhibit different binding ability (Fig. 1C). The region between the TM domain and the CAD/SOAR domain of STIM1 has been suggested to have an inhibitory effect on Orai binding (Butorac et al., 2019; Fahrner et al., 2014; Korzeniowski et al., 2010; Yang et al., 2012). Consistently, the precipitates by 3NT or 3CT contained much less STIM1 when residues 233–341 of human STIM1 were included (Fig. 1C, lanes 4 and 7). Similarly, reduced binding of the Orai peptides was observed with a STIM1 fragment of residues 310–531, although to a lesser extent (Fig. 1C, lanes 5 and 8). Thus, the pull-down assay we developed here is valid for investigating STIM1-Orai interactions *in vitro*.

The interactions were further analyzed by biolayer interferometry (BLI). Biotinylated peptides, including 3CT and 3NT, were individually immobilized to streptavidin sensor surface, and incubated with increasing concentrations (0.125–4 µM) of purified STIM1 (residues 342–531). The association and disassociation of STIM1 to the sensor, which influenced the thickness of the layer on the sensor tip, was monitored by BLI as an interference wavelength shift. The affinity between STIM1 and 3CT peptide was determined as ∼0.4 µM, whereas that of 3NT was ∼0.6 µM (Fig. 1D,E). Consistent with this, STIM1 exhibited a weaker affinity for 1CT (∼2.6 µM) than 3CT (Fig. S1C).

Sequential interactions with Orai3-NT and Orai3-CT

Next, we tested whether STIM1 contacts the NT and CT of Orai in a stepwise manner. We introduced biotin-free peptides into the pull-down assay and monitored their competition with the biotinylated peptides. As expected, when unlabeled peptides of the same type were added, they effectively reduced the co-precipitation of STIM1 (residues 342–531) with the labeled peptides (Fig. 2A, lanes 2 and 3 for 3NT, and lanes 5 and 7 for 3CT). Interestingly, the presence of 3NT drastically affected the interactions between 3CT and STIM1 (Fig. 2A, lane 6), whereas 3CT did not influence the binding of STIM1 to 3NT (Fig. 2A, lane 4). These results suggest that the interactions with Orai-NT prevent STIM1 from binding to Orai-CT, supporting the notion that the contact occurs in a sequential order: STIM1 to the CT first and NT second.

The differentiated interactions between STIM1 and Orai peptides were also analyzed by BLI. When STIM1 (4 µM) was pre-incubated with an excess amount of 3NT (80 µM), it still interacted with immobilized Bio-3CT on the sensor, but quickly dissociated

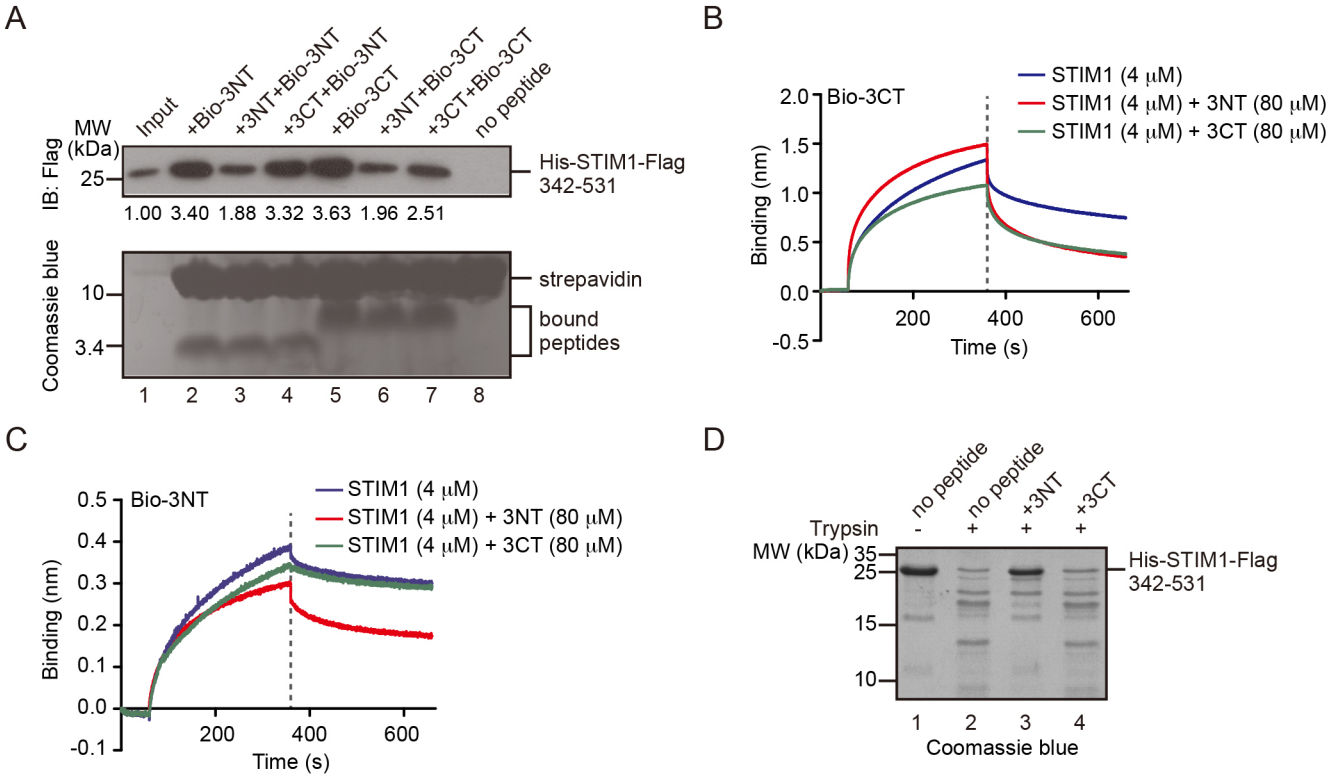

Fig. 2. Sequential interactions between STIM1 and Orai3. (A) Unlabeled Orai3 NT and CT peptides were pre-incubated with STIM1 (residues 342–531) for 1 h at 4°C, then the pull-down assay was performed. 2% of the input and 50% of the precipitates were loaded. The relative levels of co-precipitated STIM1 were quantified using Gel-Pro analyzer software. Data are representative of three biological repeats. (B,C) Unlabeled 3NT and 3CT were pre-incubated with STIM1, and then BLI analysis was performed with sensors coated with Bio-3CT (B) and Bio-3NT (C). Data are representative of two biological repeats. (D) STIM1 (residues 342–531) was incubated with the Orai3 peptide for 1 h at 4°C and then subjected to trypsin treatment. All samples were analyzed by SDS-PAGE and stained with Coomassie Blue. Data are representative of three biological repeats.

Journal of Cell Science

Journal of Cell Science (2020) 133, jcs239491. doi:10.1242/jcs.239491

(Fig. 2B). These results suggest that 3NT and 3CT may engage STIM1 simultaneously, but 3NT-bound STIM1 has a much-decreased affinity for 3CT. As expected, 3CT-loaded STIM1 has decreased binding to immobilized Bio-3CT (Fig. 2B). Similarly, 3NT-loaded STIM1 has decreased binding to immobilized Bio-3NT, but 3CT-loaded STIM1 associated and disassociated with Bio-3NT in a similar curve to STIM1 alone (Fig. 2C). STIM1 or unlabeled peptide-saturated STIM1 has undifferentiated interactions to biocytin-coated reference sensor (Fig. S1D). In addition, no heterotypic or homotypic interaction was detected between 3NT and 3CT (Fig. S1E), ruling out the possibility that competition is directly between the peptides. Collectively, these results indicate that 3CT-bound STIM1 is fully capable of interacting with 3NT, but 3NT-bound STIM1 loses affinity for 3CT.

The weaker interaction of the CT with the STIM1-Orai-NT complex than STIM1 alone implies that STIM may adopt different conformations when binding to different termini of Orai channels. To probe this possibility, we performed a trypsin-protection assay. Without peptides, STIM1 molecules were readily digested into at least five lower-molecular-mass species (Fig. 2D, lane 2). When 3NT was added, the majority of the STIM1 proteins were protected from trypsin cleavage (Fig. 2D, lane 3). Such protection was not seen, however, when 3CT was present (Fig. 2D, lane 4). These results suggest that Orai-NT shields different regions on STIM1 to Orai-CT, and Orai-NT likely triggers a conformational change in STIM1 that prevents it from stably contacting Orai-CT.

Interaction determinants in Orai3-NT

To narrow down the critical elements in Orai-NT for STIM1 interactions, we performed a pull-down assay using mutated 3NT peptides (Fig. 3A). Residues pointing away from the ion-passing face were primarily chosen, as they are most likely accessible to STIM1. When R52 or R53 was mutated to alanine, co-precipitation of STIM1 was drastically reduced (Fig. 3B, lanes 3–4). Consistently, the R52A/R53A double mutant exhibited no detectable interaction with STIM1 (Fig. 3B, lane 5). It has been reported that a triple mutant (L81A/S82A/K85A) of Orai1-NT peptide affects interaction with STIM1 (Gudlur et al., 2014). We made an equivalent mutant in 3NT (L56A/S57A/K60A) and found a reduced affinity, as expected (Fig. 3C, lane 6). Individual mutation of the locus revealed that the defects were mainly caused by L56A (Fig. 3C, lanes 3–5). These results suggest that a basic region in Orai3-NT plays a prominent role in recruiting STIM1.

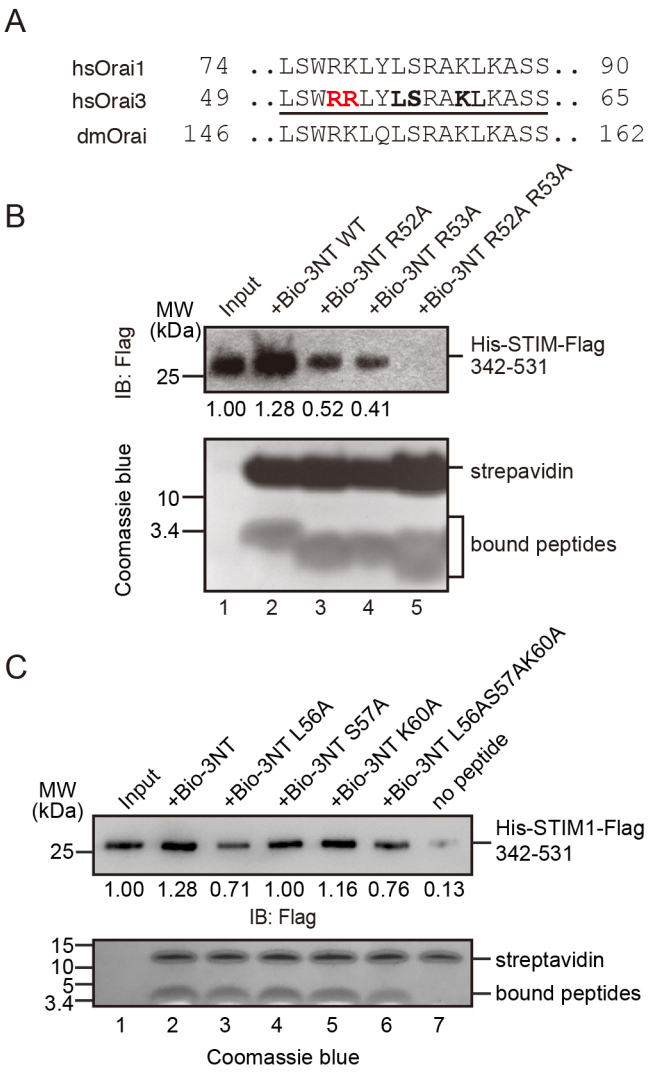

Fig. 3. Determinants of Orai3 N termini for STIM1 interactions. (A) Sequence alignment of Orai-NT. Residues in bold are mutated and the ones that substantially affect interactions with STIM1 are highlighted in red. hs, *Homo sapiens*; dm, *Drosophila melanogaster*. (B,C) Peptide pull-down assay of STIM1 (residues 342–531) with wild-type and mutant Orai3-NT peptides. The relative levels of STIM1 were quantified using Gel-Pro analyzer software. Data are representative of three biological repeats.

Interaction determinants in Orai3-CT

To dissect the critical regions in Orai-CT for the STIM1-Orai complex, we performed a pull-down assay using mutated 3CT peptides (Fig. 4A). First, we noticed that TM4 and Orai-CT adopt a continuously helical pattern in the dmOrai structure, but the helix links at a conserved 'RSLV' motif, part of which was previously termed the Orai nexus (Zhou et al., 2016) (Fig. 4A, red). When this motif was deleted from the 3CT peptide, binding to STIM1 was largely compromised (Fig. 4B, lane 3). Similarly, V271A retained nearly no interaction with STIM1 (Fig. 4B, lane 7). S269A reduced its ability to interact with STIM1 (Fig. 4B, lane 5), whereas R268A and L270A showed little change compared to wild type (Fig. 4B, lanes 4 and 6).

Next, we tested whether hydrophobic residues in Orai3-CT are important. Five candidates were found in addition to the already tested L270 and V271 (Fig. 4A, green). As expected, L282 (equivalent to L273 in Orai1) appeared to be critical (Fig. 4C, lane 3). We found that L285A affected STIM1 interactions similar to L282A (Fig. 4C, lane 4), L288A and L292A affected STIM1 to a lesser extent (Fig. 4C, lanes 5 and 6), and V295A had no effect (Fig. 4C, lane 7). The same changes were seen when leucines were replaced with serines (Fig. S2A,B). To assess whether the mutations used here affect the helical propensity of the peptides, we used circular dichroism (CD) measurements. Wild-type 3CT was less helical in aqueous buffer but exhibited signature peaks for an α-helix in the presence of trifluoroethanol (TFE) (Fig. S2C). Similarly, both L282A and L282S exhibited an α-helical pattern with TFE (Fig. S2C). These results suggest that the affected interactions seen with mutated peptides are less likely due to altered secondary structures.

Next, we tested polar residues in 3CT. Given that STIM1 possesses many basic residues on the surface, we mutated all negatively charged residues in 3CT (Fig. 4A, cyan). Most of the mutations had little impact on the interaction (Fig. 4D), except E281 and E291, and substitution of these residues with lysine mildly reduced the interaction (Fig. 4D, lanes 4 and 7). When other polar residues, including N286, Q289, and Q293, were mutated, no

Journal of Cell Science (2020) 133, jcs239491. doi:10.1242/jcs.239491

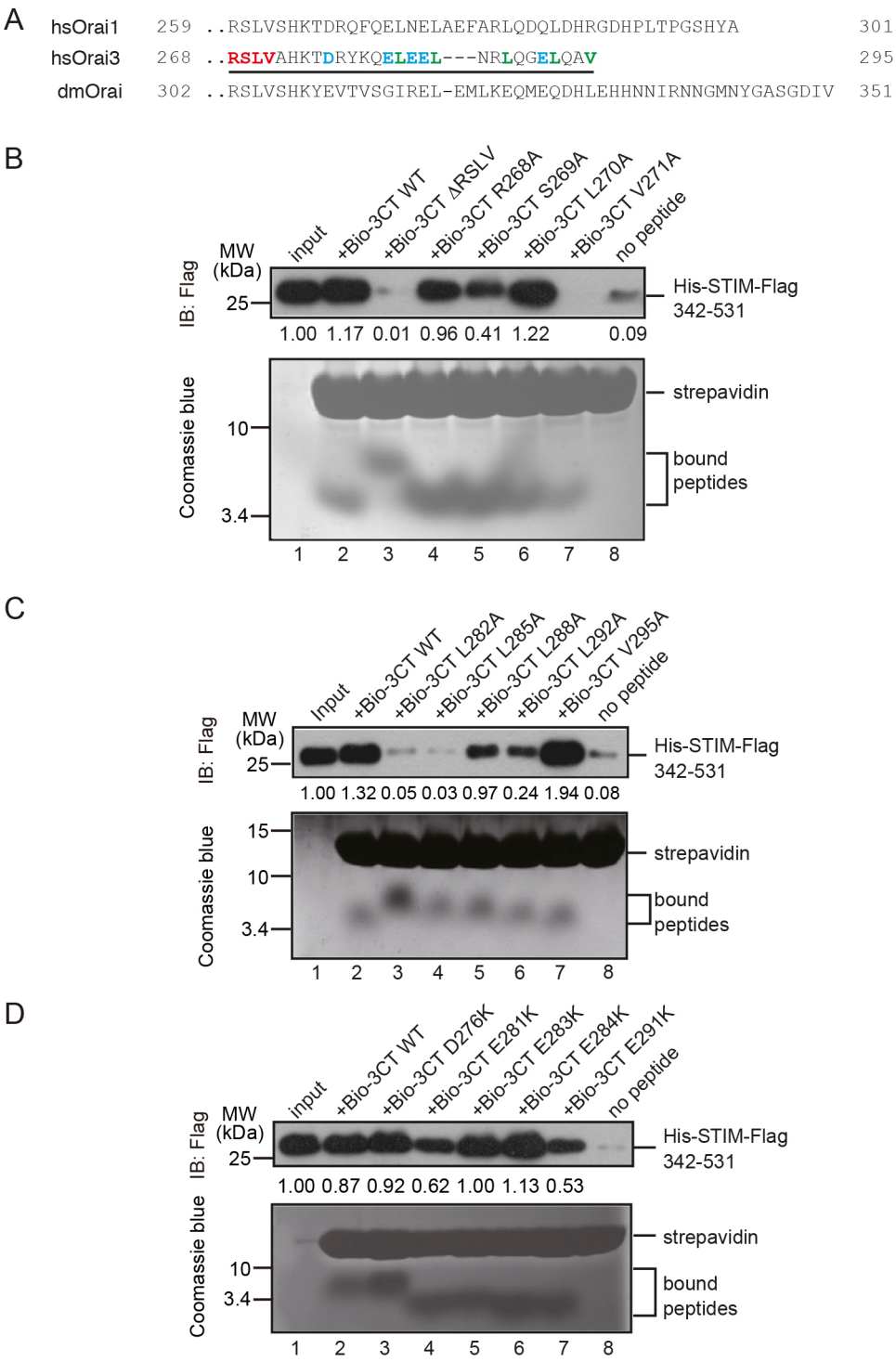

Fig. 4. Determinants of Orai3 C termini for STIM1 interactions. (A) Sequence alignment of Orai-CT with RSLV motif highlighted in red, hydrophobic residues in green and polar residues in cyan. (B) Biotinylated Orai3-CT wild-type and RSLV motif mutant peptides (RSLV deletion and point mutant peptides) were assayed for binding to STIM1 342–531 in streptavidin-based peptide pull-down assay. 5% of the input and 50% of the precipitates were loaded. The relative levels of STIM1 were quantified using Gel-Pro analyzer software. Data are representative of three biological repeats. (C) As in B, but hydrophobic residues mutated 3CT peptides were assayed. (D) As in B, but polar residues mutated 3CT peptides were assayed.

obvious changes in STIM1 co-precipitation were seen (Fig. S2A,D). Collectively, these results suggest that Orai-CT-mediated STIM interactions rely mostly on hydrophobic residues. In summary, V271, L282, and L285 are the most important, whereas S269, E281, E291 and L292 also contribute, but are less critical.

Key residues identified in 3CT are almost all conserved in 1CT. Thus, it is puzzling as to why 3CT binds to STIM1 more efficiently than 1CT. We noticed that Orai1 is longer than Orai3 at the CT (Fig. S3A). To test whether binding elements are missing from the 1CT peptide, we extended it by adding six more residues at the CT. However, the longer peptide still exhibited a weak interaction with STIM1 (Fig. S3B, lane 6). We also found that three residues (AEF) are inserted after L276 of 1CT (equivalent to L285 of 3CT) compared to 3CT. To examine this, we truncated 3CT at L285 (3CT short, Fig. S3A). Even though only E291 and L292 in the missing part can partially regulate STIM1 interactions, 3CT short nearly diminished STIM1 binding (Fig. S3B, lane 3). Interestingly, when the AEF motif was deleted from 1CT, the mutated peptide had increased interaction with STIM1 compared to wild type (Fig. S3B, lane 7). Conversely, when the AEF motif was added to 3CT, the

Journal of Cell Science (2020) 133, jcs239491. doi:10.1242/jcs.239491

mutated peptides lost affinity for STIM1 (Fig. S3B, lane 4). Thus, the AEF insertion in 1CT reduced interactions with STIM1, likely by shifting the positions of key residues in the CT.

Tests of STIM1-Orai interactions in cells

Next, we tested the key components identified here in a cellular context. To compare Orai1-CT and Orai3-CT, we generated a chimeric construct by replacing the CT of Orai1 with that of Orai3 (Orai1-3CT). Myc-tagged wild-type or chimeric Orai1 was co-transfected with Flag-STIM1 into human embryonic kidney (HEK) 293T cells. When Flag-STIM1 was precipitated by anti-Flag agarose, the levels of co-precipitated Myc-Orai1 were probed by western blotting. As expected, wild-type STIM1 successfully pulled down Orai, and the interactions were enhanced when cells were treated with thapsigargin (TG) to induce SOCE (Fig. 5A). Similar co-immunoprecipitation was performed with STIM1 and Orai1-3CT. More Orai co-precipitated in this case, with or without TG treatment (Fig. 5A). We also measured TG-evoked SOCE in 293T cells. SOCE was elevated when Orai1 and STIM1 were co-expressed, but not when GFP or STIM1 alone was expressed (Fig. 5B,C). SOCE was further increased, to a little but reproducible extent, when Orai1-3CT and STIM1 were co-transfected (Fig. 5B,C). Expression levels and the intracellular localization of these proteins were verified in HEK293T cells (Fig. S4A,B). Finally, we tested whether the STIM1 fragment (residues 342–531) we used in the pull-down assay is sufficient to constitutively active Orai. As expected, cells co-transfected with Flag-STIM1 342-531 and Orai1-GFP (see Fig. S4E for expression levels) exhibited elevated Ca^{2+} influx upon the addition of 2 mM Ca^{2+} in the medium. The influx was further increased when Orai1-3CT was transfected (Fig. S4C). Notably, ectopically expressed STIM1 fragment nicely colocalized with Orai-GFP, suggesting an efficient association (Fig. S4D). These findings suggest that Orai3-CT likely conveys stronger binding to STIM1 than Orai1-CT, which can lead to increased SOCE.

To verify key residues in Orai and to avoid interference from endogenous Orai, we co-transfected wild-type or mutant Orai1-3CT with GFP-STIM1 into Orai-deleted HEK293T cells [triple knockout (TKO) of Orai 1–3; see Fig. S5A for expression and localization]. As shown previously (Zheng et al., 2018b), TKO cells exhibited minimal TG-evoked SOCE (Fig. 6A,B). When R77 and K78 in Orai1-NT (equivalent to R52 and R53 in Orai3-NT) were mutated, the SOCE of GFP-STIM1 co-transfected cells was reduced (Fig. 6A, B). Similarly, when L282 or V271 (Orai3 numbering kept for Orai1-3CT) was substituted with alanine, the SOCE was decreased (Fig. 6). E281K and E291K caused further reduction, close to background level (Fig. 6). In contrast, S269A, which mildly affected STIM1 interaction *in vitro*, caused no significant reduction (Fig. 6).

It has been suggested that NT mutants of Orai, particularly Orai1 R77A and K78A, directly block channel function (Liu et al., 2019). We therefore tested the double mutant in a constitutively active 'ANSGA' channel (Zhou et al., 2016). Consistently, the ANSGA channel is more active than the wild-type channel, but the R77A K78A mutations abolished the activation by the ANSGA channel (Fig. S5B–E). Our results suggest that these conserved basic residues in Orai-NT likely support channel activation purely by intra-Orai interactions.

We also tested whether 'AEF' deletion in the CT of Orai1 or corresponding insertion in Orai1-3CT affects SOCE. Consistent with interaction analysis, Orai1ΔAEF conveyed more efficient SOCE and Orai1-3CT+AEF displayed opposite effect (Fig. S3C–E). Taken together, these results confirm the role of key residues in SOCE.

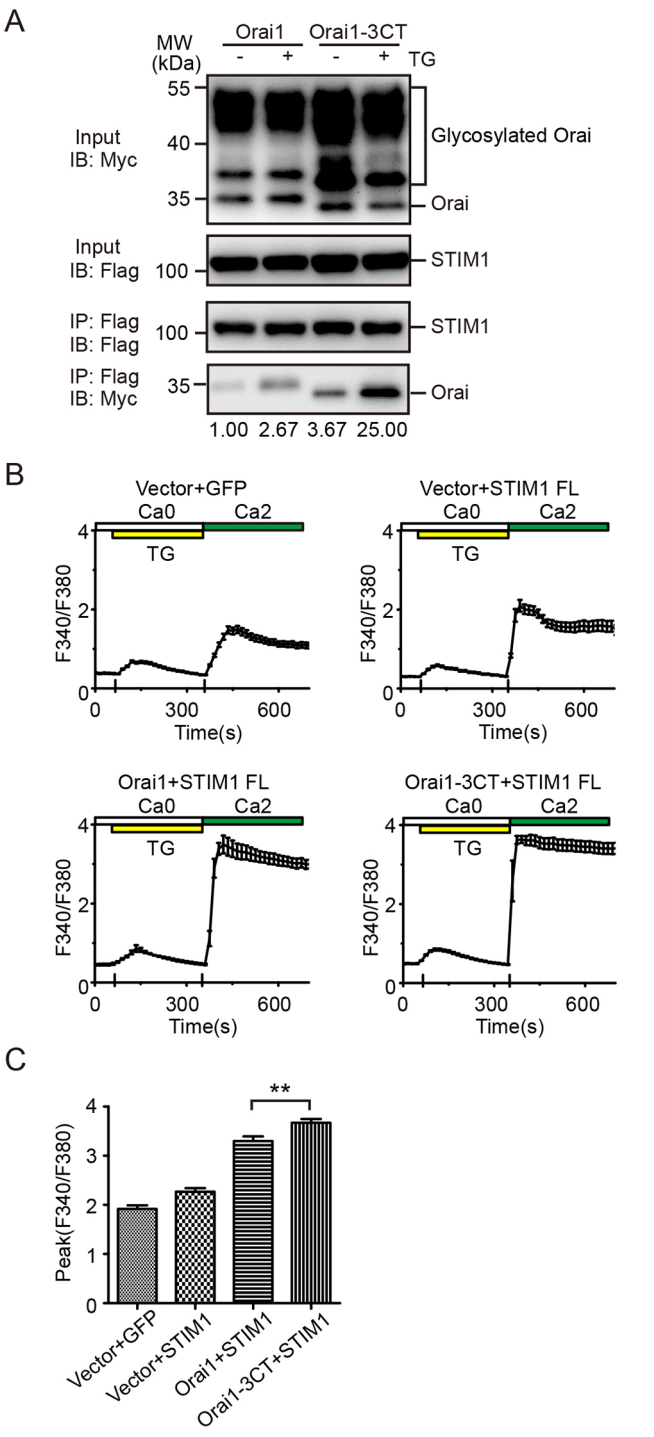

Fig. 5. Comparison of Orai1-CT and Orai3-CT in cells. (A) Co-immunoprecipitation of Myc-Orai1 or Myc-Orai1-3CT with Flag-STIM1 in transiently transfected HEK293T cells. Input represents 5% of the total cell extract used for immunoprecipitation. Input samples and Flag-tagged immunoprecipitation were blotted with anti-Flag and anti-Myc antibodies. The relative levels of precipitated Orai were normalized to precipitated STIM1 correspondingly. Data are representative of three biological repeats. (B) Fura-2 ratiometric constitutive Ca^{2+} entry responses following thapsigargin (TG) stimulation in HEK293T cells transfected with Myc vector+GFP (negative control; n=11 cells), Myc vector+GFP-STIM1 (n=10), Myc-Orai1+GFP-STIM1 (n=13) or Myc-Orai1-3CT+GFP-STIM1 (n=11). (C) Averaged peak Ca^{2+} entry responses represented in B. Vector+GFP, n=102; Vector+STIM1, n=92; Orai1+STIM1, n=104; Orai1-3CT+STIM1, n=93. **P<0.01 by two-tailed Student's t-test. Error bars denote s.e.m. from at least three independent experiments.

Journal of Cell Science (2020) 133, jcs239491. doi:10.1242/jcs.239491

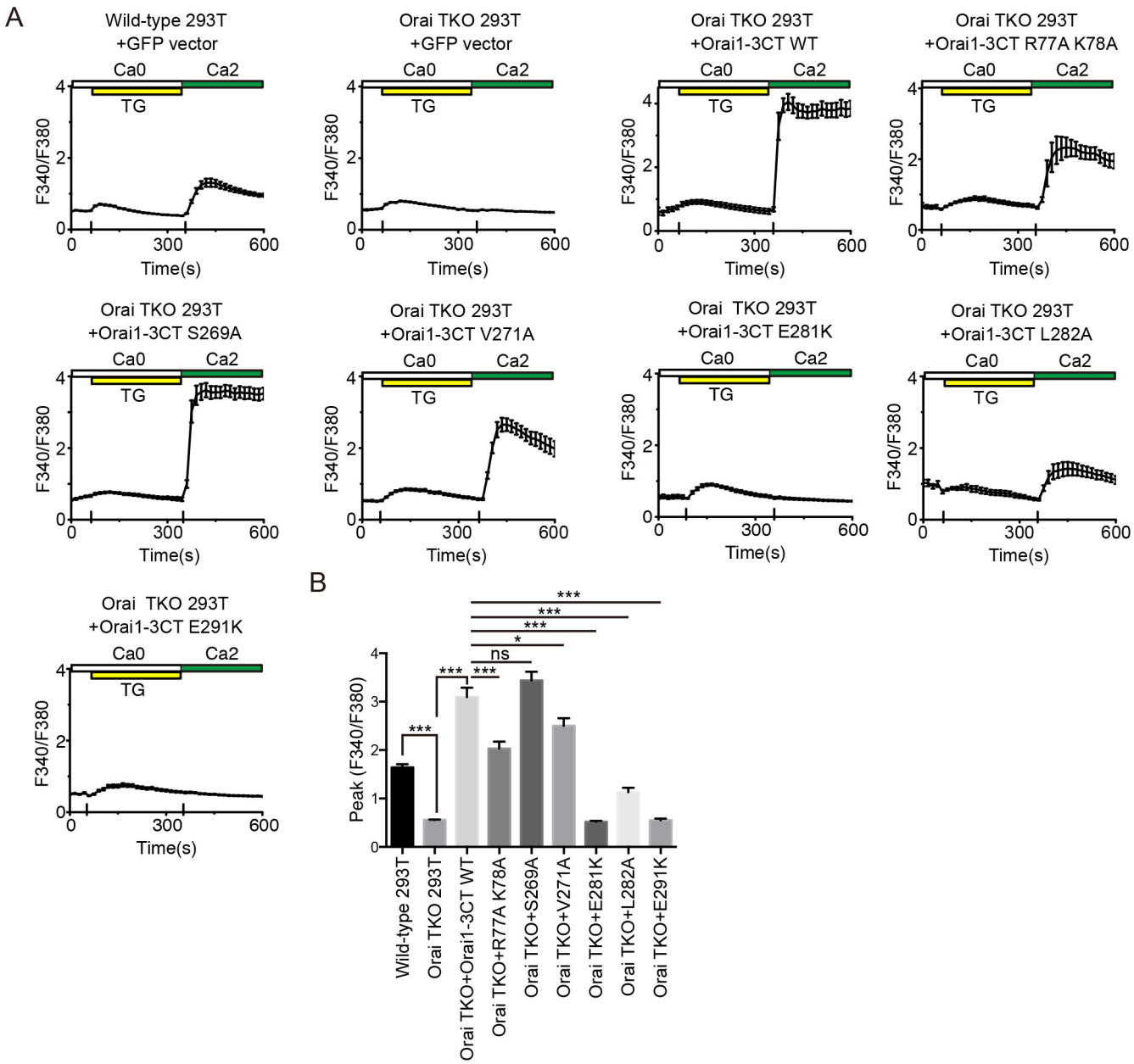

Fig. 6. Key residues for STIM1-Orai interactions tested in cells. (A) Fura-2 ratiometric constitutive Ca^{2+} entry responses following TG stimulation in wild-type HEK293T cells transfected with GFP vector (*n*=13 cells), Orai triple knockout (TKO) HEK293T cells transfected with GFP vector (*n*=11), and Orai TKO HEK293T cells co-transfected with Myc-Orai1-3CT mutations (WT, *n*=7; R77A K78A, *n*=7; S269A, *n*=9; V271A, *n*=12; E281K, *n*=9; L282A, *n*=10; E291K, *n*=10) and GFP-STIM1. (B) Averaged peak Ca^{2+} entry responses were collected from corresponding HEK293T cells (wild-type 293T transfected with GFP vector, *n*=37; Orai TKO HEK293T transfected with GFP vector, *n*=29; Orai TKO HEK293T co-transfected with GFP-STIM1 and WT Orai1-3CT, *n*=27; R77A K78A, *n*=35; S269A, *n*=22; V271A, *n*=28; E281K, *n*=30; L282A, *n*=24; E291K, *n*=30). ns, not significant; **P*<0.05, ****P*<0.001 by two-tailed Student's *t*-test. Error bars are defined as s.e.m. from at least three independent experiments.

DISCUSSION

We developed a pull-down assay to assess direct interactions between STIM and Orai. The STIM1 fragments we used contain the well-known regions for Orai binding, with no engineered mutations for purification optimization. However, Orai is represented by synthetic peptides matching its NT and CT. Structural analysis has revealed that the termini of dmOrai exist as relatively independent helices (Hou et al., 2012; Liu et al., 2019). The peptides appear to retain the helical propensity seen in full-length molecules. Therefore, the pull-down assay likely unveils details about direct binding with high fidelity.

By using this assay, we systematically probed interface determinants for the STIM1-Orai3 complex, and most identified residues in Orai3 are conserved in Orai1. We confirmed the complex-forming roles of some previously proposed residues, including Orai1 R77/K78 (Orai3 R52/R53) (Bergsmann et al., 2011; Frischauf et al., 2009, 2011) in the NT, and Orai1 V262 (Orai3 V271) (Zhou et al., 2016), L273 (Orai3 L282) (Bergsmann et al., 2011; Li et al., 2011; Muik et al., 2008) and L276 (Orai3 L285) (Bergsmann et al., 2011; Navarro-Borelly et al., 2008) in the CT. We also identified new determinants of STIM-Orai interaction, such as Orai1 S260 (Orai3 S269), E272 (Orai3 E281), Q285 (Orai3 E291) and L286 (Orai3 L292).

Journal of Cell Science (2020) 133, jcs239491. doi:10.1242/jcs.239491

The NT of Orai, including the essential region termed extended transmembrane Orai1 N-terminal (ETON) (Derler et al., 2013), forms the ion pore of the channel along with TM1 of Orai. Movement of this region likely impacts Ca^{2+} influx and, therefore, gates the channel. We showed that STIM1 physically contacts Orai-NT, specifically at two tandem basic residues (R52/R53 in Orai3, equivalent to R77/K78 in Orai1). We confirmed that Orai3 L56 (equivalent to Orai1 L81A) also plays a role. Residues further towards the lipid bilayer, even though they do not face the ion pore, are less likely reached by STIM1. For example, Orai1 K85 has previously been shown to be critical for SOCE (Lis et al., 2010), but does not contribute to the STIM1 interaction as tested here. Mutations of these residues likely alter pore properties through a changed association with surrounding TMs (Yamashita et al., 2020; Yeung and Prakriya, 2018; Yeung et al., 2019). Interestingly, the key STIM1-interacting residues, R77/K78 in Orai1-NT, directly impact channel opening. Whether they still play a role in channel gating through STIM1 binding remains to be investigated.

The CT of Orai mediates the CC type of interaction with STIM1. It adopts a helical configuration and connects to TM4 with a flexible linker, and as such is also termed TM4 extension (TM4E). Interestingly, the linker can be transformed into part of the long TM4 helix in the open state of dmOrai (Hou et al., 2018; Liu et al., 2019). We included the linker region in our Orai-CT peptides. The linker and a few subsequent residues were defined as the STIM1 binding site nexus, which may exert an impact on TM3 with L261 and subsequently gate the channel (Zhou et al., 2016). Consistently, we found that Orai1 V262 (Orai3 V271) and S260 (Orai3 S269) are involved in binding to STIM1, but L261 (Orai3 L270) is not. Following the linker, two leucines (L273/L276 in Orai1 and L282/L285 in Orai3) are well established for STIM1 interaction. In the closed-state dmOrai structure, these two hydrophobic residues appear at the CT dimer interface. Therefore, they may contribute to STIM1 recruitment indirectly. However, the dynamics of Orai-CT CC may be needed for STIM1-mediated activation (Muik et al., 2008; Tirado-Lee et al., 2015), and they are indeed exposed in the open-state structures. Thus, these key leucines may also serve as a binding site. Furthermore, we identified L292 of Orai3 as a partial determinant for STIM1 binding. This residue is near the very end of Orai3; it less likely supports potential dimerization of Orai-CT and more likely engages STIM1 directly.

The structures of both CC1-CC2 and CC2-CC3 of STIM1 have been determined (Stathopulos et al., 2013; Yang et al., 2012). An Orai1-CT peptide is included in the structure of CC1-CC2, and CC2 makes most contacts with it. However, the CC2-CC3 structure, which is equivalent to SOAR/CAD, contains no Orai fragment. It is speculated that a polybasic tip between CC2 and CC3 can serve as an Orai1 binding site. Our results demonstrate that the polybasic region is dispersible for interacting with STIM1. Rearrangements between STIM1 CCs are likely responsible for activating STIM1, as the presence of CC1 reduces the affinity of STIM1 for both NT and CT Orai peptides.

As previously demonstrated, the NT and CT peptides of Orai both bind to purified STIM1 (Gudlur et al., 2014; Park et al., 2009; Zhou et al., 2010). Importantly, we discovered that pre-incubation of Orai-NT with STIM1 compromises further interactions with Orai-CT. In addition, NT-bound and CT-bound STIM1 exhibit a differential tryptic pattern, and the two termini likely bind to different regions of STIM1. Even though further confirmation in a full-length context is needed, these findings confirm the following model, which was also proposed recently (Palty et al., 2017): activated STIM1 approaches Orai channels first via Orai-CT; apposing STIM1 then attaches to Orai-NT. It is also consistent with the structure-based gating model, in which conformational changes in TM4 (Orai-CT) are transduced to the opening of TM1 (Orai-NT) (Liu et al., 2019). Given the mystery of STIM-Orai binding stoichiometry, it is not clear whether each STIM1 has to go through a CT-NT transition.

Our pull-down assay revealed that the CT of Orai1 is less competent than that of Orai3 in interacting with STIM1. The key difference is a three-residue insertion in Orai1. When both CTs form helices, insertion adds an extra turn for Orai1-CT, which in turn projects the remaining sequences further away from the STIM1 binding site or becomes less helical prone. Orai3 does not possess the insertion and is predicted to bind to STIM1 more strongly than Orai1. This sequence difference between Orai1 and Orai3 has been explored previously in the context of SOCE induction. Deletion of three residues in Orai1 enhances SOCE (Frischauf et al., 2009), but insertion of them in Orai3 also increases its activity (Alansary et al., 2015). Interestingly, when the same insertion was done in the context of Orai1-3CT chimera, a decrease in SOCE was observed. These apparent discrepancies suggest that binding affinity between STIM and different Orai-CTs is evolutionarily set for the pore-forming part of the matching Orai channels. Orai1 channel possess a weaker STIM1-binding CT but a higher SOCE capability compared to Orai2 and Oria3; altercations that enhance STIM1 recruitment elevate Orai1-mediated SOCE. Conversely, Orai2 and Orai3 have a relatively higher affinity for STIM1 but lower levels of SOCE (Frischauf et al., 2009); decreased interactions with STIM1 help to boost channel activities. Collectively, tight binding may not always be beneficial for subsequent channel activation. The roles of different Orai channels have yet to be clarified. It is certainly possible that different cell types demand different levels and kinetics of SOCE. Thus, differential expression of Orai channels could be used to fine tune SOCE.

MATERIALS AND METHODS

Plasmids and reagents

Human STIM1 fragments (residues 233–531, residues 310–531, residues 342–531) were cloned into the pET-28a vector with a Flag tag at the C terminus. The generation of GFP-STIM1 (Roos et al., 2005), Myc-Orai1 (Zhang et al., 2008) and Myc-Orai1-3CT (Zhang et al., 2008) chimera were described previously. Orai1-GFP and Orai1-3CT-GFP were PCR amplified from Myc-Orai1, and Myc-Orai1-3CT and cloned into pEGFP-N1 vectors. Flag-STIM1 (residues 342–531) was PCR amplified from GFP-STIM1 and cloned into pcDNA4TO vector with a Flag tag at the N terminus. All point mutations were created by exchanging the corresponding codons using the QuikChange XL Site-Directed Mutagenesis Kit (Agilent Technologies).

Cell culture and transfection

HEK293T cells (Invitrogen) and Orai1–3 TKO HEK293T cells (Zheng et al., 2018b) were maintained in Dulbecco's modified Eagle medium (DMEM; Corning) supplemented with 10% fetal bovine serum (Hyclone) at 37°C with 5% CO_2. All cells were recently authenticated and tested for contamination. Cells were transfected using Lipofectamine 3000 (Invitrogen) based on the manufacturer's instructions.

Protein expression and purification

STIM1 protein was expressed in the *Escherichia coli* strain Rosetta (Novagen). Cells were grown at 37°C in LB medium with 50 mg/l kanamycin at 37°C to an optical density at a wavelength of 600 nm of 0.6. Expression was induced by addition of 0.5 mM isopropyl-β-D-thiogalactoside for 12 h at 24°C. The cells were harvested and lysed by sonication in buffer containing 50 mM Tris-HCl (pH 8.0), 300 mM NaCl, 2 mM β-mercaptoethanol and protease inhibitor cocktail (Roche). The His-tagged recombinant proteins were isolated by Ni-NTA chromatography (Qiagen) and further purified by ion-exchange chromatography (GE Healthcare). All of the Orai peptides were synthetized by GL Biochem (Shanghai) Ltd.

Pull-down assay

Biotin-labeled Orai peptides (20 µM) were immobilized on Strep-Tactin Sepharose (Qiagen) and incubated with purified STIM1 proteins (2 µM) in 500 µl PBS (pH 7.4) for 1 h at 4°C. The beads were washed three times with 1 ml PBS containing 1% Triton X-100 to eliminate non-specific binding. The precipitated proteins were eluted with boiling SDS and analyzed by SDS-PAGE and western blotting.

In Ni-NTA-agarose pull-down assay, purified His-tagged STIM1 (residues 342–531) (4 µM) was mixed with unlabeled or biotinylated Orai3 peptides (40 µM) in 500 µl PBS, and Ni-NTA-agarose beads were added. After an incubation for 1 h at 4°C, the beads were pelleted and washed three times with 1 ml PBS containing 1% Triton X-100 to eliminate non-specific binding. The precipitated proteins were eluted with boiling SDS and analyzed by SDS-PAGE.

BLI

BLI experiments were performed using an Octet96 (FortéBio, Menlo Park, CA) using streptavidin sensors. Proteins used in BLI experiments were buffer exchanged into the assay buffer [50 mM Tris-HCl (pH 8.0), 300 mM NaCl, 0.02% Tween 20]. Assays were performed in 96-well plates at 30°C; 200-µl volumes were used in each well. Biotinylated Orai peptides (5 µg/ml) were loaded onto sensors for 300 s followed by baseline measurements in binding buffer for 60 s. Association was measured by dipping sensors into solutions of analyte protein and was followed by moving sensors to buffer only to monitor dissociation. Coated and uncoated reference sensors were both blocked with a solution of 5 µM biocytin for 60 s at 30°C. Data analysis was performed with the FortéBio Data Analysis 7.0 software. Binding was fitted to a global 1:1 association-then-dissociation model.

For BLI-based competition experiments, STIM1 protein (4 µM) was pre-incubated with label-free Orai peptides (80 µM) for 1 h at 4°C. Association and dissociation of samples to coated and uncoated reference sensors were measured for 300 s.

Trypsin protection assay

STIM1 (residues 342–531; 10 µg) was incubated with the indicated Orai peptide (20 µM) in a total reaction volume of 40 µl for 1 h at 4°C, and then incubated with 2 ng trypsin for 5 min at 37°C. The reaction was terminated by the addition of SDS buffer and the samples were resolved by SDS-PAGE and stained with Coomassie Blue.

Immunoprecipitation

Transfected HEK293T cells (24 h) were washed with PBS, and treated with Ca2 or Ca0 (Zhou et al., 2014) plus 1 µM TG (Merck Millipore) for 10 min at room temperature. Cells were washed and lysed in 50 mM Tris-HCl (pH 7.5), 150 mM NaCl, 1% Triton X-100 and protease inhibitors. Lysates were spun at 12,000 rpm for 10 min and the supernatant incubated with anti-Flag M2 agarose beads (Sigma-Aldrich). Lysates and immunoprecipitates were subjected to SDS-PAGE.

Western blotting

Samples were resolved by SDS-PAGE and analyzed by standard western blotting. The immunoblot was incubated with the indicated primary antibodies for 1 h at room temperature or overnight at 4°C, followed by horseradish peroxidase (HRP)-linked secondary antibodies (KPL) for 1 h. Immunoreactivity was detected by ECL Western Blotting Substrate (Pierce). The following commercial primary antibodies were used: rabbit anti-Flag (Sigma-Aldrich, F7425; 1:2000), rabbit anti-Myc (Sigma-Aldrich, C3956; 1:2000), rabbit anti-GFP (Thermo Fisher Scientific, A-11122; 1:2000) and mouse anti-tubulin (Thermo Fisher Scientific, MA1-19400; 1:2000).

Band densities were quantified using Gel-Pro Analyzer version 4.0 (Media Cybernetics).

Immunofluorescence and confocal microscopy

HEK293T cells were fixed in 4% paraformaldehyde for 20 min at room temperature and permeabilized with 0.1% Triton X-100 in PBS for 10 min. Fixed cells were blocked and incubated with rabbit anti-Myc antibody (Sigma-Aldrich, C3956; 1:500) or rabbit anti-Flag antibody (Sigma-Aldrich, F7425; 1:500) for 1 h at room temperature, and then goat anti-rabbit Alexa Fluor 568 (Thermo Fisher Scientific, A-11036; 1:1000) for 1 h. All images were taken on a Zeiss LSM700 confocal microscope.

Single-cell $[Ca^{2+}]_i$ imaging

Ratiometric single-cell intracellular Ca^{2+} {$[Ca^{2+}]_i$} imaging was performed on an IX-81 microscope (Olympus)-based system as described previously (Li et al., 2017). Transfected HEK293T cells were incubated in DMEM containing 2 µM Fura-2 AM (Invitrogen) at 37°C for 45 min. Data were acquired by MetaFluor software (Universal Imaging) and analyzed using OriginPro 8 software. Data are expressed as means±s.e.m.

Statistical analysis

Data analysis was performed using GraphPad Prism 5. Data are expressed as means±s.e.m. Significance in each group was determined using Student's *t*-test considering $P<0.05$.

Acknowledgements

We thank Dr Youjun Wang for kindly providing the Orai TKO cell line and helpful comments on the manuscript, and Dr Alicia Prater for proofreading.

Competing interests

The authors declare no competing or financial interests.

Author contributions

Conceptualization: S.L.Z., J.H., Q.W.; Methodology: L.N., F.W., J.L., J.H.; Validation: L.N., F.W., K.L.; Formal analysis: L.N., F.W., K.L., J.L., S.L.Z.; Investigation: L.N., F.W., K.L., J.L., J.H., Q.W.; Data curation: L.N., F.W., J.L., S.L.Z.; Writing - original draft: J.H.; Writing - review & editing: L.N., J.H., Q.W.; Visualization: L.N., F.W., K.L.; Supervision: S.L.Z., J.H., Q.W.; Project administration: S.L.Z., J.H., Q.W.; Funding acquisition: J.H., Q.W.

Funding

J.H. is supported by the Ministry of Science and Technology of the People's Republic of China [2016YFA0500201] and the National Natural Science Foundation of China [91854202 and 31630020]. F.W. is supported by the National Natural Science Foundation of China [81702639]. Q.W. is supported by startup funds from Tianjin Medical University.

Supplementary information

Supplementary information available online at
http://jcs.biologists.org/lookup/doi/10.1242/jcs.239491.supplemental

Peer review history

The peer review history is available online at
https://jcs.biologists.org/lookup/doi/10.1242/jcs.239491.reviewer-comments.pdf

References

Alansary, D., Bogeski, I. and Niemeyer, B. A. (2015). Facilitation of Orai3 targeting and store-operated function by Orai1. *Biochim. Biophys. Acta Mol. Cell Res.* **1853**, 1541-1550. doi:10.1016/j.bbamcr.2015.03.007

Baba, Y., Hayashi, K., Fujii, Y., Mizushima, A., Watarai, H., Wakamori, M., Numaga, T., Mori, Y., Iino, M., Hikida, M. et al. (2006). Coupling of STIM1 to store-operated Ca2+ entry through its constitutive and inducible movement in the endoplasmic reticulum. *Proc. Natl. Acad. Sci. USA* **103**, 16704-16709. doi:10.1073/pnas.0608358103

Bergsmann, J., Derler, I., Muik, M., Frischauf, I., Fahrner, M., Pollheimer, P., Schwarzinger, C., Gruber, H. J., Groschner, K. and Romanin, C. (2011). Molecular determinants within N terminus of Orai3 protein that control channel activation and gating. *J. Biol. Chem.* **286**, 31565-31575. doi:10.1074/jbc.M111.227546

Böhm, J. and Laporte, J. (2018). Gain-of-function mutations in STIM1 and ORAI1 causing tubular aggregate myopathy and Stormorken syndrome. *Cell Calcium* **76**, 1-9. doi:10.1016/j.ceca.2018.07.008

Butorac, C., Muik, M., Derler, I., Stadlbauer, M., Lunz, V., Krizova, A., Lindinger, S., Schober, R., Frischauf, I., Bhardwaj, R. et al. (2019). A novel STIM1-Orai1 gating interface essential for CRAC channel activation. *Cell Calcium* **79**, 57-67. doi:10.1016/j.ceca.2019.02.009

Calloway, N., Owens, T., Corwith, K., Rodgers, W., Holowka, D. and Baird, B. (2011). Stimulated association of STIM1 and Orai1 is regulated by the balance of PtdIns(4,5)P-2 between distinct membrane pools. *J. Cell Sci.* **124**, 2602-2610. doi:10.1242/jcs.084178

Covington, E. D., Wu, M. M. and Lewis, R. S. (2010). Essential role for the CRAC activation domain in store-dependent oligomerization of STIM1. *Mol. Biol. Cell* **21**, 1897-1907. doi:10.1091/mbc.e10-02-0145

Derler, I., Plenk, P., Fahrner, M., Muik, M., Jardin, I., Schindl, R., Gruber, H. J., Groschner, K. and Romanin, C. (2013). The extended transmembrane Orai1 N-terminal (ETON) region combines binding interface and gate for Orai1 activation by STIM1. *J. Biol. Chem.* **288**, 29025-29034. doi:10.1074/jbc.M113.501510

Derler, I., Butorac, C., Krizova, A., Stadlbauer, M., Muik, M., Fahrner, M., Frischauf, I. and Romanin, C. (2018). Authentic CRAC channel activity requires STIM1 and the conserved portion of the Orai N terminus. *J. Biol. Chem.* **293**, 1259-1270. doi:10.1074/jbc.M117.812206

Enomoto, M., Nishikawa, T., Back, S. I., Ishiyama, N., Zheng, L., Stathopulos, P. B. and Ikura, M. (2019). Coordination of a single calcium ion in the EF-hand maintains the off state of the stromal interaction molecule luminal domain. *J. Mol. Biol.* **432**, 367-383. doi:10.1016/j.jmb.2019.10.003

Fahrner, M., Muik, M., Schindl, R., Butorac, C., Stathopulos, P., Zheng, L., Jardin, I., Ikura, M. and Romanin, C. (2014). A coiled-coil clamp controls both conformation and clustering of stromal interaction molecule 1 (STIM1). *J. Biol. Chem.* **289**, 33231-33244. doi:10.1074/jbc.M114.610022

Feske, S., Gwack, Y., Prakriya, M., Srikanth, S., Puppel, S.-H., Tanasa, B., Hogan, P. G., Lewis, R. S., Daly, M. and Rao, A. (2006). A mutation in Orai1 causes immune deficiency by abrogating CRAC channel function. *Nature* **441**, 179-185. doi:10.1038/nature04702

Feske, S., Picard, C. and Fischer, A. (2010). Immunodeficiency due to mutations in ORAI1 and STIM1. *Clin. Immunol.* **135**, 169-182. doi:10.1016/j.clim.2010.01.011

Frischauf, I., Muik, M., Derler, I., Bergsmann, J., Fahrner, M., Schindl, R., Groschner, K. and Romanin, C. (2009). Molecular determinants of the coupling between STIM1 and Orai channels: differential activation of Orai1-3 channels by a STIM1 coiled-coil mutant. *J. Biol. Chem.* **284**, 21696-21706. doi:10.1074/jbc.M109.018408

Frischauf, I., Schindl, R., Bergsmann, J., Derler, I., Fahrner, M., Muik, M., Fritsch, R., Lackner, B., Groschner, K. and Romanin, C. (2011). Cooperativeness of Orai cytosolic domains tunes subtype-specific gating. *J. Biol. Chem.* **286**, 8577-8584. doi:10.1074/jbc.M110.187179

Gudlur, A., Quintana, A., Zhou, Y., Hirve, N., Mahapatra, S. and Hogan, P. G. (2014). STIM1 triggers a gating rearrangement at the extracellular mouth of the ORAI1 channel. *Nat. Commun.* **5**, 5164. doi:10.1038/ncomms6164

Gudlur, A., Zeraik, A. E., Hirve, N., Rajanikanth, V., Bobkov, A. A., Ma, G., Zheng, S., Wang, Y., Zhou, Y., Komives, E. A. et al. (2018). Calcium sensing by the STIM1 ER-luminal domain. *Nat. Commun.* **9**, 4536. doi:10.1038/s41467-018-06816-8

Hirve, N., Rajanikanth, V., Hogan, P. G. and Gudlur, A. (2018). Coiled-coil formation conveys a STIM1 signal from ER lumen to cytoplasm. *Cell Rep.* **22**, 72-83. doi:10.1016/j.celrep.2017.12.030

Hogan, P. G. and Rao, A. (2015). Store-operated calcium entry: mechanisms and modulation. *Biochem. Biophys. Res. Commun.* **460**, 40-49. doi:10.1016/j.bbrc.2015.02.110

Hogan, P. G., Lewis, R. S. and Rao, A. (2010). Molecular basis of calcium signaling in lymphocytes: STIM and ORAI. *Annu. Rev. Immunol.* **28**, 491-533. doi:10.1146/annurev.immunol.021908.132550

Hou, X., Pedi, L., Diver, M. M. and Long, S. B. (2012). Crystal structure of the calcium release-activated calcium channel Orai. *Science* **338**, 1308-1313. doi:10.1126/science.1228757

Hou, X., Burstein, S. R. and Long, S. B. (2018). Structures reveal opening of the store-operated calcium channel Orai. *eLife* **7**, e36758. doi:10.7554/eLife.36758

Korzeniowski, M. K., Popovic, M. A., Szentpetery, Z., Varnai, P., Stojilkovic, S. S. and Balla, T. (2009). Dependence of STIM1/Orai1-mediated calcium entry on plasma membrane phosphoinositides. *J. Biol. Chem.* **284**, 21027-21035. doi:10.1074/jbc.M109.012252

Korzeniowski, M. K., Manjarres, I. M., Varnai, P. and Balla, T. (2010). Activation of STIM1-Orai1 involves an intramolecular switching mechanism. *Sci. Signal.* **3**, ra82. doi:10.1126/scisignal.2001122

Lacruz, R. S. and Feske, S. (2015). Diseases caused by mutations in ORAI1 and STIM1. *Ann. N. Y. Acad. Sci.* **1356**, 45-79. doi:10.1111/nyas.12938

Li, Z., Liu, L., Deng, Y., Ji, W., Du, W., Xu, P., Chen, L. and Xu, T. (2011). Graded activation of CRAC channel by binding of different numbers of STIM1 to Orai1 subunits. *Cell Res.* **21**, 305-315. doi:10.1038/cr.2010.131

Li, J., Yan, B., Si, H. J., Peng, X., Zhang, S. Y. L. and Hu, J. J. (2017). Atlastin regulates store-operated calcium entry for nerve growth factor-induced neurite outgrowth. *Sci. Rep.* **7**, 43490. doi:10.1038/srep43490

Liou, J., Kim, M. L., Heo, W. D., Jones, J. T., Myers, J. W., Ferrell, J. E., Jr and Meyer, T. (2005). STIM is a Ca2+ sensor essential for Ca2+-store-depletion-triggered Ca2+ influx. *Curr. Biol.* **15**, 1235-1241. doi:10.1016/j.cub.2005.05.055

Liou, J., Fivaz, M., Inoue, T. and Meyer, T. (2007). Live-cell imaging reveals sequential oligomerization and local plasma membrane targeting of stromal interaction molecule 1 after Ca2+ store depletion. *Proc. Natl. Acad. Sci. USA* **104**, 9301-9306. doi:10.1073/pnas.0702866104

Lis, A., Zierler, S., Peinelt, C., Fleig, A. and Penner, R. (2010). A single lysine in the N-terminal region of store-operated channels is critical for STIM1-mediated gating. *J. Gen. Physiol.* **136**, 673-686. doi:10.1085/jgp.201010484

Liu, X., Wu, G., Yu, Y., Chen, X., Ji, R., Lu, J., Li, X., Zhang, X., Yang, X. and Shen, Y. (2019). Molecular understanding of calcium permeation through the open Orai channel. *PLoS Biol.* **17**, e3000096. doi:10.1371/journal.pbio.3000096

Luik, R. M., Wu, M. M., Buchanan, J. A. and Lewis, R. S. (2006). The elementary unit of store-operated Ca2+ entry: local activation of CRAC channels by STIM1 at ER-plasma membrane junctions. *J. Cell Biol.* **174**, 815-825. doi:10.1083/jcb.200604015

Lunz, V., Romanin, C. and Frischauf, I. (2019). STIM1 activation of Orai1. *Cell Calcium* **77**, 29-38. doi:10.1016/j.ceca.2018.11.009

Ma, G., Wei, M., He, L., Liu, C., Wu, B., Zhang, S. L., Jing, J., Liang, X., Senes, A., Tan, P. et al. (2015). Inside-out Ca^{2+} signalling prompted by STIM1 conformational switch. *Nat. Commun.* **6**, 7826. doi:10.1038/ncomms8826

Muik, M., Frischauf, I., Derler, I., Fahrner, M., Bergsmann, J., Eder, P., Schindl, R., Hesch, C., Polzinger, B., Fritsch, R. et al. (2008). Dynamic coupling of the putative coiled-coil domain of ORAI1 with STIM1 mediates ORAI1 channel activation. *J. Biol. Chem.* **283**, 8014-8022. doi:10.1074/jbc.M708898200

Muik, M., Fahrner, M., Derler, I., Schindl, R., Bergsmann, J., Frischauf, I., Groschner, K. and Romanin, C. (2009). A cytosolic homomerization and a modulatory domain within STIM1 C terminus determine coupling to ORAI1 channels. *J. Biol. Chem.* **284**, 8421-8426. doi:10.1074/jbc.C800229200

Navarro-Borelly, L., Somasundaram, A., Yamashita, M., Ren, D., Miller, R. J. and Prakriya, M. (2008). STIM1-Orai1 interactions and Orai1 conformational changes revealed by live-cell FRET microscopy. *J. Physiol. Lond.* **586**, 5383-5401. doi:10.1113/jphysiol.2008.162503

Palty, R., Fu, Z. and Isacoff, E. Y. (2017). Sequential steps of CRAC channel activation. *Cell Rep.* **19**, 1929-1939. doi:10.1016/j.celrep.2017.05.025

Park, C. Y., Hoover, P. J., Mullins, F. M., Bachhawat, P., Covington, E. D., Raunser, S., Walz, T., Garcia, K. C., Dolmetsch, R. E. and Lewis, R. S. (2009). STIM1 clusters and activates CRAC channels via direct binding of a cytosolic domain to Orai1. *Cell* **136**, 876-890. doi:10.1016/j.cell.2009.02.014

Prakriya, M. and Lewis, R. S. (2015). Store-operated calcium channels. *Physiol. Rev.* **95**, 1383-1436. doi:10.1152/physrev.00020.2014

Prakriya, M., Feske, S., Gwack, Y., Srikanth, S., Rao, A. and Hogan, P. G. (2006). Orai1 is an essential pore subunit of the CRAC channel. *Nature* **443**, 230-233. doi:10.1038/nature05122

Putney, J. W. (1986). A model for receptor-regulated calcium entry. *Cell Calcium* **7**, 1-12. doi:10.1016/0143-4160(86)90026-6

Roos, J., DiGregorio, P. J., Yeromin, A. V., Ohlsen, K., Lioudyno, M., Zhang, S., Safrina, O., Kozak, J. A., Wagner, S. L., Cahalan, M. D. et al. (2005). STIM1, an essential and conserved component of store-operated Ca2+ channel function. *J. Cell Biol.* **169**, 435-445. doi:10.1083/jcb.200502019

Soboloff, J., Rothberg, B. S., Madesh, M. and Gill, D. L. (2012). STIM proteins: dynamic calcium signal transducers. *Nat. Rev. Mol. Cell Biol.* **13**, 549-565. doi:10.1038/nrm3414

Stathopulos, P. B., Schindl, R., Fahrner, M., Zheng, L., Gasmi-Seabrook, G. M., Muik, M., Romanin, C. and Ikura, M. (2013). STIM1/Orai1 coiled-coil interplay in the regulation of store-operated calcium entry. *Nat. Commun.* **4**, 2963. doi:10.1038/ncomms3963

Tirado-Lee, L., Yamashita, M. and Prakriya, M. (2015). Conformational changes in the Orai1 C-terminus evoked by STIM1 binding. *PLoS ONE* **10**, e0128622. doi:10.1371/journal.pone.0128622

Vig, M., Beck, A., Billingsley, J. M., Lis, A., Parvez, S., Peinelt, C., Koomoa, D. L., Soboloff, J., Gill, D. L., Fleig, A. et al. (2006). CRACM1 multimers form the ion-selective pore of the CRAC channel. *Curr. Biol.* **16**, 2073-2079. doi:10.1016/j.cub.2006.08.085

Walsh, C. M., Chvanov, M., Haynes, L. P., Petersen, O. H., Tepikin, A. V. and Burgoyne, R. D. (2010). Role of phosphoinositides in STIM1 dynamics and store-operated calcium entry. *Biochem. J.* **425**, 159-168. doi:10.1042/BJ20090884

Wu, M. M., Buchanan, J. A., Luik, R. M. and Lewis, R. S. (2006). Ca2+ store depletion causes STIM1 to accumulate in ER regions closely associated with the plasma membrane. *J. Cell Biol.* **174**, 803-813. doi:10.1083/jcb.200604014

Yamashita, M., Navarro-Borelly, L., McNally, B. A. and Prakriya, M. (2007). Orai1 mutations alter ion permeation and Ca2+-dependent fast inactivation of CRAC channels: evidence for coupling of permeation and gating. *J. Gen. Physiol.* **130**, 525-540. doi:10.1085/jgp.200709872

Yamashita, M., Ing, C. E., Yeung, P. S., Maneshi, M. M., Pomes, R. and Prakriya, M. (2020). The basic residues in the Orai1 channel inner pore promote opening of the outer hydrophobic gate. *J. Gen. Physiol.* **152**, e201912397. doi:10.1085/jgp.201912397

Yang, X., Jin, H., Cai, X., Li, S. and Shen, Y. (2012). Structural and mechanistic insights into the activation of Stromal interaction molecule 1 (STIM1). *Proc. Natl. Acad. Sci. USA* **109**, 5657-5662. doi:10.1073/pnas.1118947109

Yeromin, A. V., Zhang, S. L., Jiang, W., Yu, Y., Safrina, O. and Cahalan, M. D. (2006). Molecular identification of the CRAC channel by altered ion selectivity in a mutant of Orai. *Nature* **443**, 226-229. doi:10.1038/nature05108

Yeung, P. S.-W. and Prakriya, M. (2018). The exquisitely cooperative nature of Orai1 channel activation. *J. Gen. Physiol.* **150**, 1352-1355. doi:10.1085/jgp.201812172

Yeung, P. S.-W., Yamashita, M. and Prakriya, M. (2019). Molecular basis of allosteric Orai1 channel activation by STIM1. *J. Physiol.*. doi:10.1113/JP276550

Yuan, J. P., Zeng, W., Dorwart, M. R., Choi, Y.-J., Worley, P. F. and Muallem, S. (2009). SOAR and the polybasic STIM1 domains gate and regulate Orai channels. *Nat. Cell Biol.* **11**, 337-343. doi:10.1038/ncb1842

Zhang, S. L., Yu, Y., Roos, J., Kozak, J. A., Deerinck, T. J., Ellisman, M. H., Stauderman, K. A. and Cahalan, M. D. (2005). STIM1 is a Ca2+ sensor that activates CRAC channels and migrates from the Ca2+ store to the plasma membrane. *Nature* **437**, 902-905. doi:10.1038/nature04147

Zhang, S. L., Yeromin, A. V., Zhang, X. H.-F., Yu, Y., Safrina, O., Penna, A., Roos, J., Stauderman, K. A. and Cahalan, M. D. (2006). Genome-wide RNAi screen of Ca2+ influx identifies genes that regulate Ca2+ release-activated Ca2+ channel activity. *Proc. Natl. Acad. Sci. USA* **103**, 9357-9362. doi:10.1073/pnas.0603161103

Zhang, S. L., Kozak, J. A., Jiang, W., Yeromin, A. V., Chen, J., Yu, Y., Penna, A., Shen, W., Chi, V. and Cahalan, M. D. (2008). Store-dependent and -independent modes regulating Ca^{2+} release-activated Ca^{2+} channel activity of human Orai1 and Orai3. *J. Biol. Chem.* **283**, 17662-17671. doi:10.1074/jbc.M801536200

Zhang, S. L., Yeromin, A. V., Hu, J., Amcheslavsky, A., Zheng, H. and Cahalan, M. D. (2011). Mutations in Orai1 transmembrane segment 1 cause STIM1-independent activation of Orai1 channels at glycine 98 and channel closure at arginine 91. *Proc. Natl. Acad. Sci. USA* **108**, 17838-17843. doi:10.1073/pnas.1114821108

Zheng, S., Ma, G., He, L., Zhang, T., Li, J., Yuan, X., Nguyen, N. T., Huang, Y., Zhang, X., Gao, P. et al. (2018a). Identification of molecular determinants that govern distinct STIM2 activation dynamics. *PLoS Biol.* **16**, e2006898. doi:10.1371/journal.pbio.2006898

Zheng, S., Zhou, L., Ma, G., Zhang, T., Liu, J., Li, J., Nguyen, N. T., Zhang, X., Li, W., Nwokonko, R. et al. (2018b). Calcium store refilling and STIM activation in STIM- and Orai-deficient cell lines. *Pflugers Arch.* **470**, 1555-1567. doi:10.1007/s00424-018-2165-5

Zhou, Y., Meraner, P., Kwon, H. T., Machnes, D., Oh-hora, M., Zimmer, J., Huang, Y., Stura, A., Rao, A. and Hogan, P. G. (2010). STIM1 gates the store-operated calcium channel ORAI1 in vitro. *Nat. Struct. Mol. Biol.* **17**, 112-116. doi:10.1038/nsmb.1724

Zhou, M.-H., Zheng, H., Si, H., Jin, Y., Peng, J. M., He, L., Zhou, Y., Muñoz-Garay, C., Zawieja, D. C., Kuo, L. et al. (2014). Stromal interaction molecule 1 (STIM1) and Orai1 mediate histamine-evoked calcium entry and nuclear factor of activated T-cells (NFAT) signaling in human umbilical vein endothelial cells. *J. Biol. Chem.* **289**, 29446-29456. doi:10.1074/jbc.M114.578492

Zhou, Y., Cai, X., Loktionova, N. A., Wang, X., Nwokonko, R. M., Wang, X., Wang, Y., Rothberg, B. S., Trebak, M. and Gill, D. L. (2016). The STIM1-binding site nexus remotely controls Orai1 channel gating. *Nat. Commun.* **7**, 13725. doi:10.1038/ncomms13725

Zhou, Y., Cai, X., Nwokonko, R. M., Loktionova, N. A., Wang, Y. and Gill, D. L. (2017). The STIM-Orai coupling interface and gating of the Orai1 channel. *Cell Calcium* **63**, 8-13. doi:10.1016/j.ceca.2017.01.001

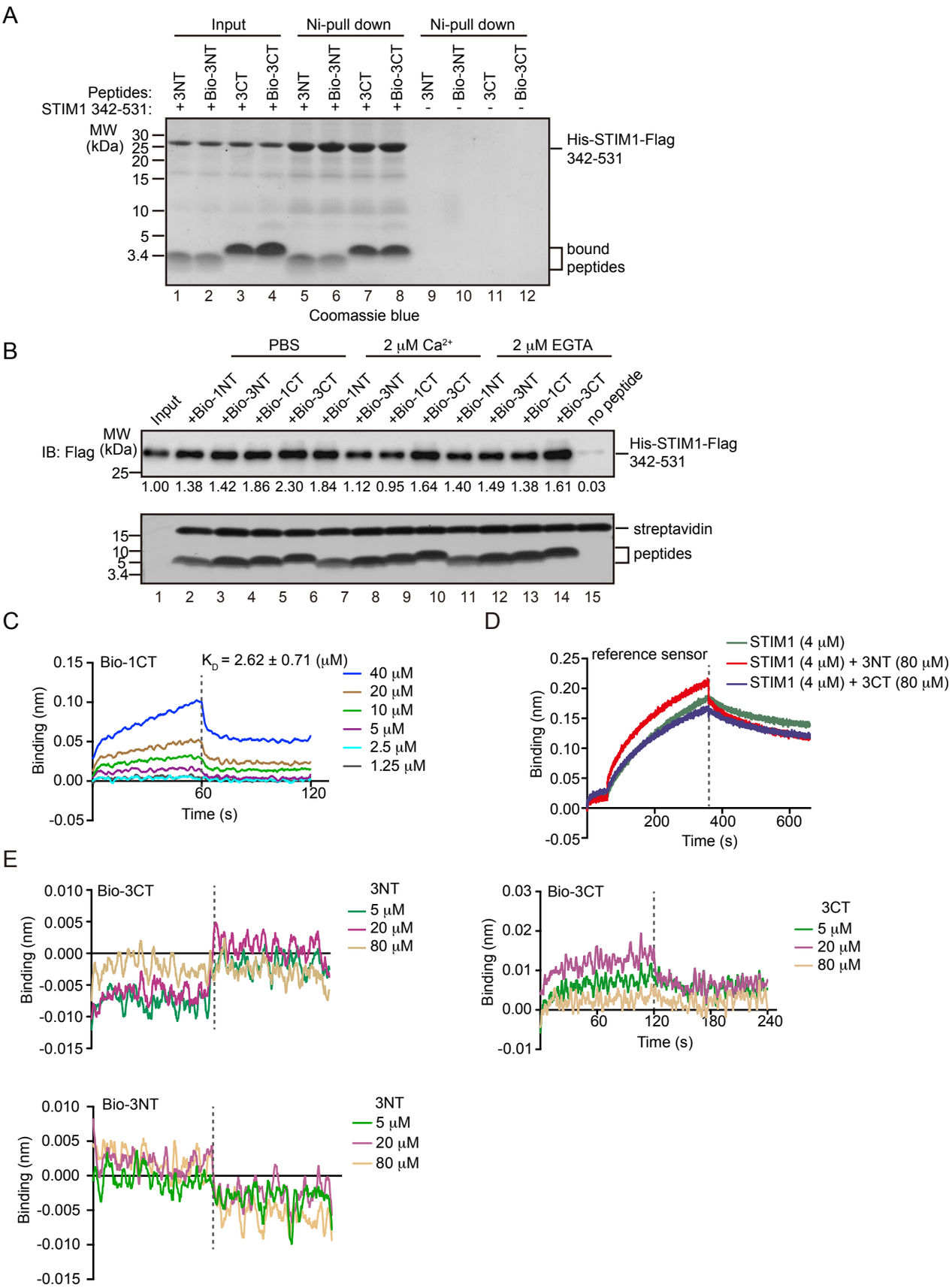

Figure S1. Interactions between STIM1 and Orai peptides. (A) Unlabeled and biotinylated Orai3 peptides (3NT and 3CT) were assayed for binding to his-STIM1 (residues 342-531) in Ni-NTA-agarose pull-down assay. Precipitates were resolved by SDS-PAGE and detected by Commassie bule staining. 1% of the input and 20% of the precipitates were loaded. (B) Biotinylated Orai peptides were assayed for binding to STIM1 (residues 342-531) in peptide pull-down assay using PBS solution, PBS buffered with 2 μM EGTA, or PBS buffered with 2 μM Ca^{2+}. Precipitates were resolved by SDS-PAGE and detected by Commassie bule staining and western blotting using anti-Flag antibodies. 5% of the input and 50% of the precipitates were loaded. The relative levels of STIM1 were quantified using the Gel-Pro analyzer software. Data are representative of three biological repeats. (C) BLI analysis of STIM1 (residues 342-531) binding to Bio-1CT. Biotinylated peptides were immobilized to streptavidin sensors. A gradient concentration of 1.25-40 μM STIM1 protein was used. Reference-subtracted raw data are rendered with fits (red lines) to a global single-state association-then-dissociation model. Association and dissociation phases were 60 s in length. Dissociation (K_D) constant was shown. Data are representative of two biological repeats. (D) STIM1 was pre-incubated with buffer, unlabeled 3NT, or unlabeled 3CT, and then the BLI analysis was performed with reference sensors. Data are representative of two biological repeats. (E) (Top) BLI analysis of unlabeled 3NT or 3CT binding to Bio-3CT. Bio-3CT was immobilized to streptavidin sensors. A gradient concentration (5 μM, 20 μM, 80 μM) of unlabeled 3NT or 3CT was used. (Bottom) BLI analysis of unlabeled 3NT to Bio-3NT. Bio-3NT was immobilized to streptavidin sensors. A gradient concentration (5 μM, 20 μM, 80 μM) of unlabeled 3NT or 3CT was used. Data are representative of two biological repeats.

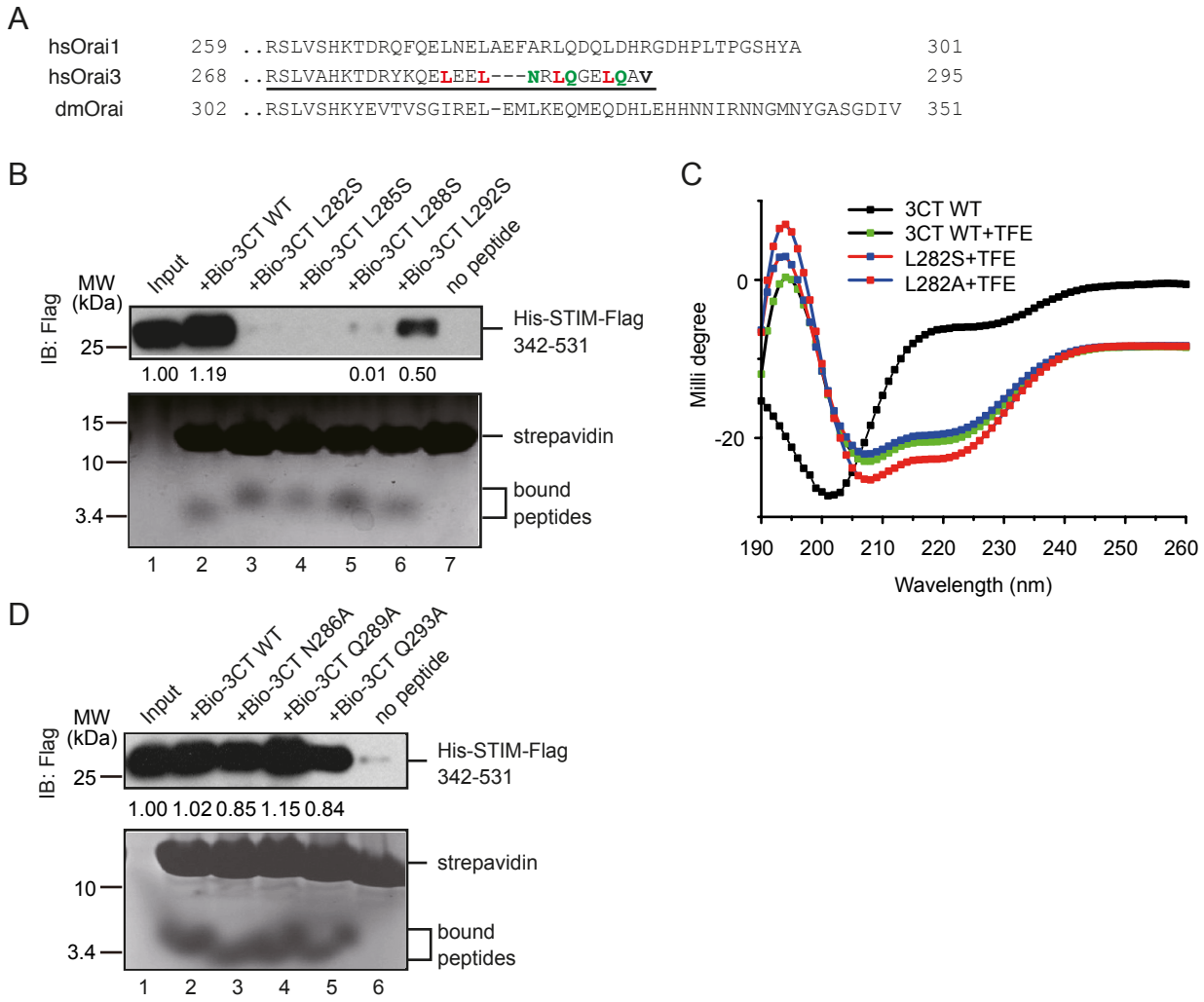

Figure S2. Hydrophobic and polar residues of Orai3-CT in STIM1 binding. (A) Sequence alignment of Orai-CT. The hydrophobic residues are highlighted in red, and polar residues are highlighted in green. (B) Biotinylated wild-type 3CT and hydrophobic residues mutated 3CT peptides were assayed for binding to STIM1 342-531 in streptavidin-based peptide pull-down assay. 5% of the input and 50% of the precipitates were loaded. The relative levels of STIM1 were quantified using the Gel-Pro analyzer software. Data are representative of three biological repeats. (C) Circular dichroism (CD) measurements of the helical propensity of the wild-type and mutant peptides in aqueous buffer or in the presence of trifluoroethanol (TFE). (D) As in (B), but with polar residues mutated.

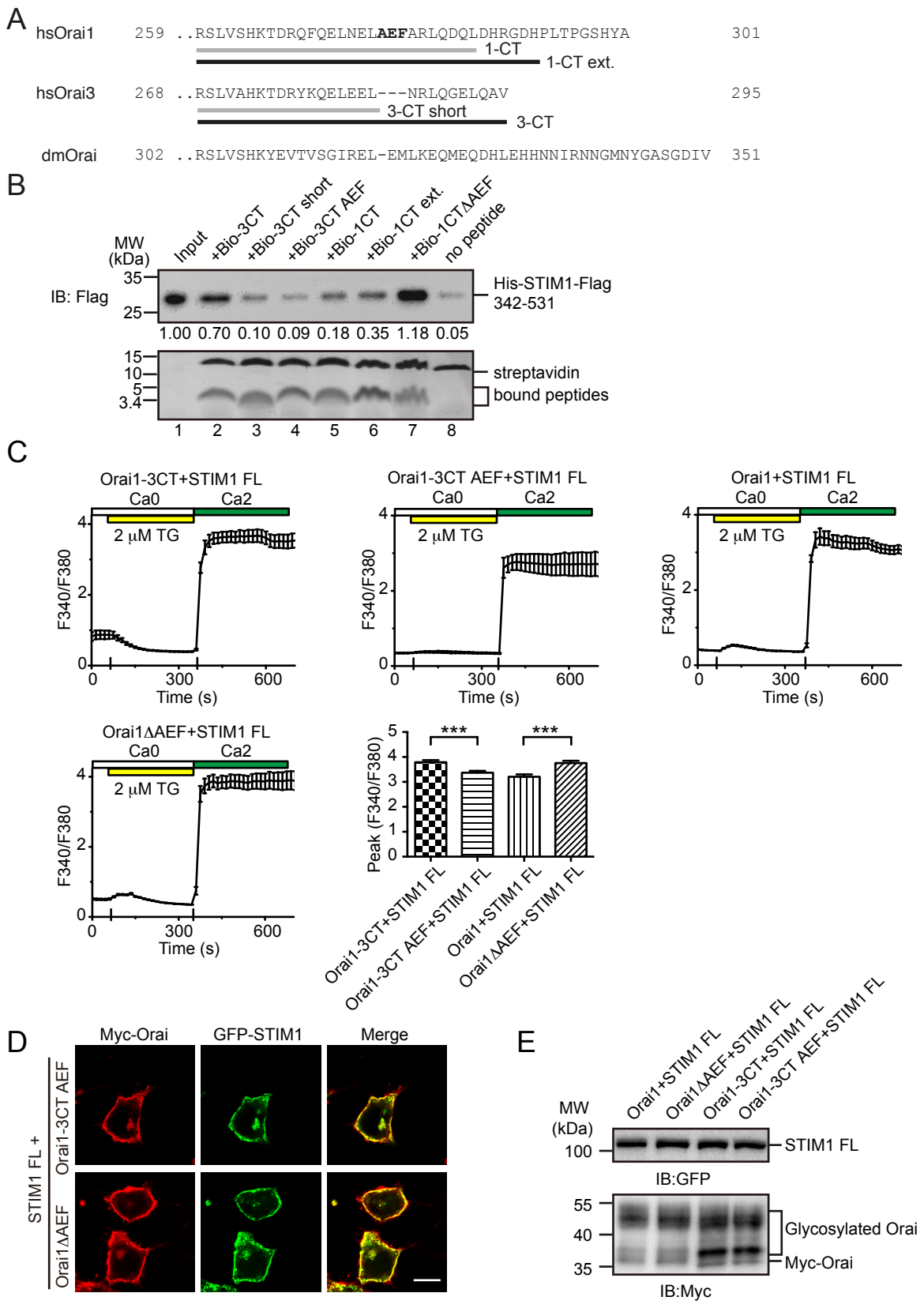

Figure S3. Orai1-CT and Orai3-CT in STIM1 binding. (A) Sequence alignment of Orai-CT. (B) Biotinylated peptides including wild-type Orai-3CT, truncated 3CT (3CT short), AEF motif insertion in 3CT (Bio-3CT+AEF), wild-type 1CT, extended 1CT (1CT ext.), AEF deletion in 1CT (1CTΔAEF) were assayed for binding to STIM1 342-531 in streptavidin-based peptide pull-down assay. 5% of the input and 50% of the precipitates were loaded. The relative levels of STIM1 were quantified using the Gel-Pro analyzer software. Data are representative of three biological repeats. (C) Fura-2 ratiometric constitutive Ca^{2+} entry responses following TG stimulation in HEK293T cells transfected with Orai1-3CT + STIM1 (n=11 cells), Orai1-3CT+AEF + STIM1 (n=7), Orai1+ STIM1 (n=9), or Orai1ΔAEF + STIM1 (n=11). Averaged peak Ca^{2+} entry responses were shown. Orai1-3CT + STIM1, n=76; Orai1-3CT+AEF + STIM1, n=70; Orai1 + STIM1, n = 65; Orai1ΔAEF + STIM1, n = 59. ***P<0.001 by two-tailed Student's *t*-test. Error bars denote s.e.m from at least three independent experiments. (D) Representative confocal images of Myc-Orai1ΔAEF and Myc-Orai1-3CT+AEF transfected HEK293T cells. Fluorescence was visualized with GFP (green) and anti-Myc (red) antibodies by indirect immunofluorescence. Scale bar, 10 μm. (E) The expression levels of proteins in (C) were determined by Western blot with anti-Myc and anti-GFP antibodies.

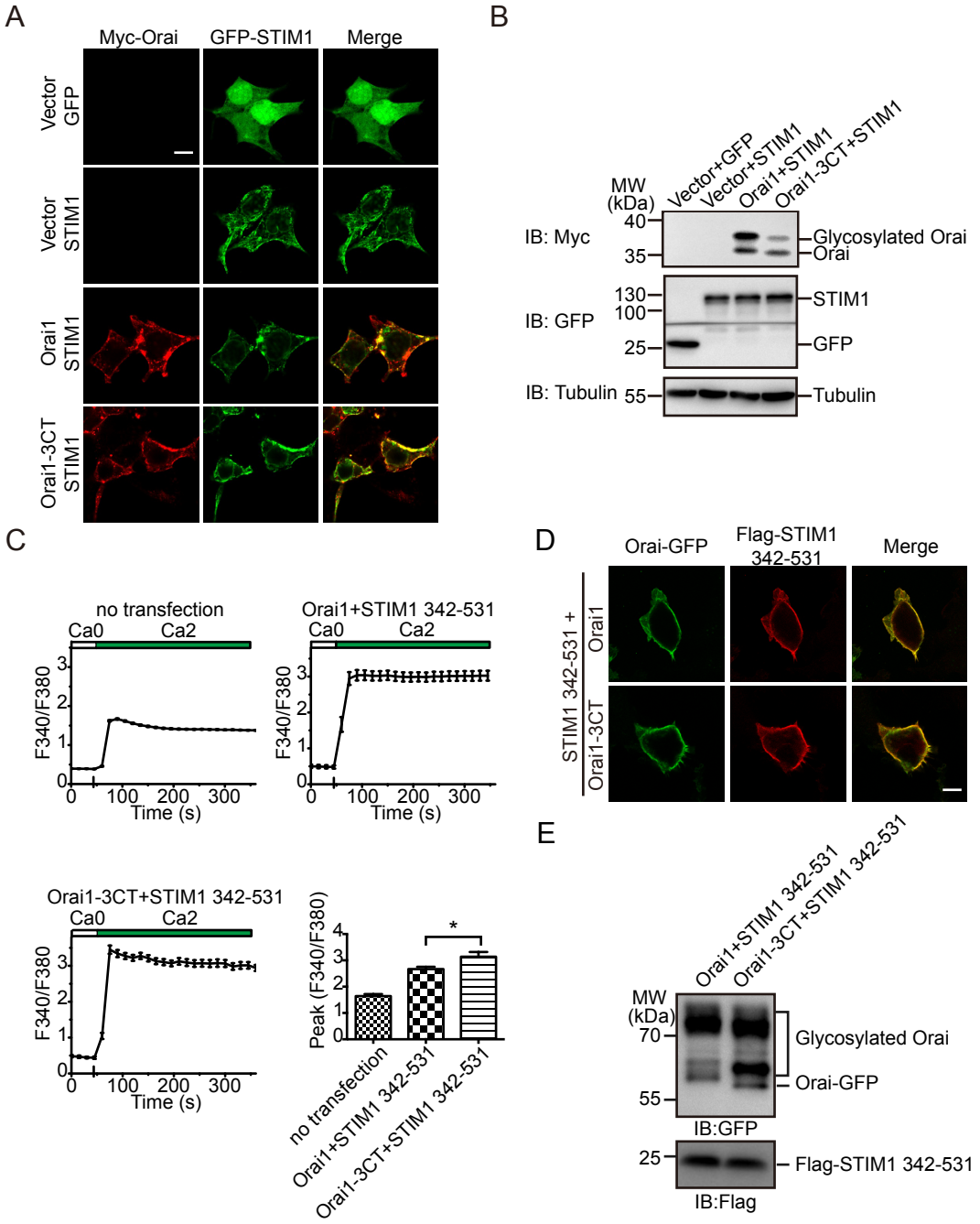

Figure S4. Expression and localization of Orai and STIM1 used in Fig. 5. (A) Representative confocal images of constructs used in Fig. 4. Fluorescence was visualized with GFP (green) and anti-Myc (red) antibodies by indirect immunofluo-rescence. Scale bar, 10 μm. (B) The expression levels of these proteins were determined by Western blot with anti-Myc and anti-GFP antibodies. Tubulin was used as a loading control. (C) Fura-2 ratiometric constitutive Ca^{2+} entry responses following TG stimulation in non-transfected HEK293T cells (n=19) or cells transfected with Orai1-GFP+Flag-STIM1 342-531 (n=11 cells), Orai1-3CT-GFP+Flag-STIM1 342-531 (n=13). Averaged peak Ca^{2+} entry responses were shown. Non-transfected HEK293T cells, n=56; Orai1+STIM1 342-531, n=53; Orai1-3CT+STIM1 342-531, n=45. **P*<0.05 by two-tailed Student's *t*-test. Error bars denote s.e.m from at least three independent experiments. (D) Representative confocal images of constructs used in C. (E) The expres-sion levels of proteins were determined by Western blot with anti-Flag and anti-GFP antibodies.

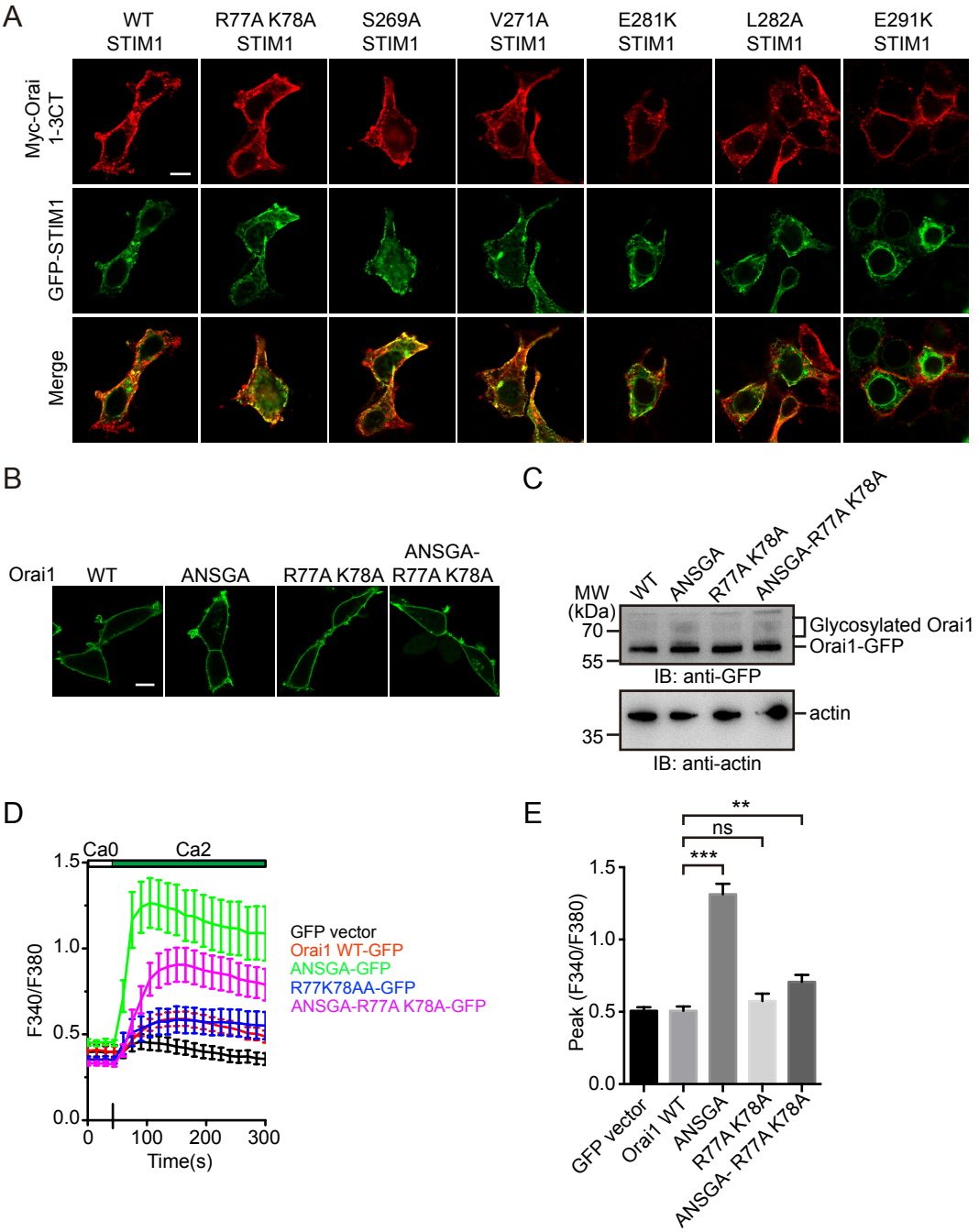

Figure S5. Expression of Orai and STIM1 used in Fig. 6. (A) Confocal images show the expression and localiza-tion of Orai1-3CT mutations. Fluorescence was visualized with GFP (green) and anti-Myc (red) antibody by indirect immunofluo-rescence. Scale bar, 10 μm. (B) Representative confocal images of HEK293T cells transfected with Orai1-GFP, Orai1 ANSGA-GFP, Orai1 R77A K78A-GFP, and Orai1 ANSGA-R77A K78A-GFP. Fluorescence was visualized with GFP. Scale bar, 10 μm. (C) The expression level of Orai1-GFP, Orai1 ANSGA-GFP, Orai1 R77A K78A-GFP, and Orai1 ANSGA-R77A K78A-GFP were determined by Western blot with anti-GFP antibody. Actin was used as a loading control. (D) Fura-2 ratiometric constitutive Ca^{2+} entry responses in Wild-type HEK293T cells transfected with GFP vector (n=10 cells), Orai1 WT-GFP (n=15), Orai1 ANSGA-GFP, n=13; Orai1 R77A K78A-GFP, n=10; Orai1 ANSGA-R77A K78A-GFP, n=15. (E) Averaged peak Ca^{2+} entry responses were collect-ed from HEK293T cells expressing GFP vector, n=50; Orai1 WT, n = 55; ANSGA, n=56; R77A K78A, n=33; ANSGA-R77A K78A, n=48. ns, not significant, $^{**}P<0.01$, $^{***}P<0.001$ by two-tailed Student's *t*-test. Error bars are defined as s.e.m from at least three independent experiments.